Title: Drosophila Ca_V2 channels harboring human migraine mutations cause synapse hyperexcitability that can be suppressed by inhibition of a Ca^{2+} store release pathway

Short Title: Drosophila models of Ca_V2 migraine mutations

Authors and Affiliations:

Douglas J. Brusich [1,4,5], Ashlyn M. Spring [1,2,6], Thomas D. James [1,3], Timothy H. Helms [1,7], C. Andrew Frank [1,2,3]

[1] – Department of Anatomy and Cell Biology, University of Iowa Carver College of Medicine, Iowa City, IA 52242

[2] – Interdisciplinary Graduate Program in Genetics, University of Iowa, Iowa City, IA 52242

[3] – Interdisciplinary Graduate Program in Neuroscience, University of Iowa, Iowa City, IA 52242

[4] – Present Address: Biology Department, Wartburg College, Waverly, IA 50677

[5] – Address as of August 2017: Human Biology, University of Wisconsin-Green Bay, Green Bay, WI 54311

[6] – Present Address: Department of Biology, University of North Carolina, Chapel Hill, NC 27599

[7] – Present Address: Department of Veterinary Biosciences, Ohio State University, Columbus, OH 43210

Address for Correspondence: C. Andrew Frank. Department of Anatomy and Cell Biology, University of Iowa Carver College of Medicine, 51 Newton Road, 1-661A. Iowa City, IA 52242. USA.

andy-frank@uiowa.edu

ABSTRACT

Gain-of-function mutations in the human $Ca_V2.1$ gene *CACNA1A* cause familial hemiplegic migraine type 1 (FHM1). To characterize cellular problems potentially triggered by $Ca_V2.1$ gains of function, we engineered mutations encoding well-known FHM1 amino-acid substitutions S218L (SL) and R192Q (RQ) into transgenes of *Drosophila melanogaster* Ca_V2/*cacophony*. We expressed the transgenes pan-neuronally. Phenotypes were mild for RQ-expressing animals. By contrast, single mutant SL- and double mutant (DM) SL, RQ-expressing animals showed severe phenotypes, including sharply decreased viability. By electrophysiology, SL- and DM-expressing neuromuscular junctions (NMJs) exhibited enhanced evoked discharges, epileptiform supernumerary discharges when single electrical pulses were applied to the motor nerves, and a dramatic increase in the amplitudes and frequencies of spontaneous miniature events. Some spontaneous events were gigantic (10-40 mV), multi-quantal events. Gigantic spontaneous events were eliminated by application of TTX – or by lowered or chelated Ca^{2+} – suggesting that giant events were elicited by spontaneous presynaptic firing. Interestingly, gain-of-function electrophysiological phenotypes were markedly lessened after genetic knockdown or mutation of Drosophila homologs of phospholipase Cβ (PLCβ), IP_3 receptor, or ryanodine receptor (RyR) – all factors known to mediate Ca^{2+} release from intracellular stores. Pharmacological inhibition of intracellular Ca^{2+} store release produced similar effects. Our data suggest inhibition of intracellular Ca^{2+} signaling could counteract hyperexcitability induced by gain-of-function $Ca_V2.1$ amino-acid substitutions.

AUTHOR SUMMARY

Prior research has demonstrated that gain-of-function mutations in a gene important for neurotransmission are known to cause migraine in humans. We attempted to mimic some of those gain-of-function mutations in a simple genetic model organism and examine neurotransmission by electrophysiology. Our findings yield potential clues as to how particular mutations may impact neurophysiology on a cellular level. We used the fruit fly *Drosophila melanogaster* and its model synapse, the neuromuscular junction (NMJ) to perform our studies. Here we document three main

advances: 1) characterization of fruit fly models harboring gain-of-function calcium channel alterations known to cause human familial hemiplegic migraine type 1 (FHM1); 2) characterization of hyperactive neurotransmission caused by one of these alterations; and 3) an ability to quell hyperactive neurotransmission by impairing intracellular Ca^{2+} store release, though both genetic and pharmacological means. Our work contributes to a broader understanding of how pathological mutations could impact cellular physiology. More generally, the utilization of genetic model organisms promises to uncover potential ways to reverse those impacts.

INTRODUCTION

Episodic neurological disorders like migraine, epilepsy, and ataxia can result from underlying ion channel dysfunctions. (1-3). For many such disorders, little is known about how aberrant channel functions affect neuronal signaling paradigms. Cell-based and model organism-based examinations of disease-causing mutations could offer insights into disease-relevant biological processes.

One Mendelian form of migraine – familial hemiplegic migraine type 1 (FHM1) – results from gain-of-function missense mutations in human *CACNA1A*, which encodes the α1 subunit of $Ca_V2.1$ (P/Q)-type calcium channels (4). Two FHM1-causing amino-acid substitutions alter highly conserved $Ca_V2.1$ α1 amino-acid residues, R192 and S218 (4, 5). The R192Q amino-acid substitution (RQ) causes "pure" FHM1, while the S218L substitution (SL) causes a severe combination of FHM1, seizures, and susceptibility to edema following head injury (4, 5). These two FHM1-causing amino-acid substitutions have been studied intensely (6), most notably in knock-in mouse models of FHM1 (7-9).

We have some information about how FHM1 mutant channels impact synaptic machinery to generate dysfunction. FHM1 knock-in mice display gain-of-function $Ca_V2.1$ phenotypes at neurons and synapses. Model synapses studied include those at the diaphragm neuromuscular junction (NMJ) (10, 11), the calyx of Held (12-14), the trigeminal sensory neuron pathway (15-17), and cortical neurons (18, 19). At the mouse NMJ, both RQ and SL increase the frequency of spontaneous excitatory potentials (10, 11). These increases in quantal frequency are dependent on mutation dose and are more

76 pronounced in SL versus RQ. SL also elicits broadening of evoked end-plate potentials at the mouse
77 NMJ (11). At the mouse calyx of Held, both substitutions result in enhanced excitatory postsynaptic
78 currents (EPSCs) (12-14), and it has been reported that SL causes an increase in the resting intracellular
79 neuronal calcium, which could be responsible for some potentiation of synapse function (12).

80 It was recently reported that tert-butyl dihydroquinone (BHQ) reverses aspects of SL-induced
81 gating dysfunction and short-term plasticity (20). For part of that study, we demonstrated that BHQ also
82 restores short-term synaptic plasticity to NMJs in fruit fly larvae expressing a transgene that encodes an
83 S161L amino-acid substitution in Drosophila Ca_V2/Cacophony – the functional equivalent of human
84 $Ca_V2.1$ S218L (20). Independent follow-up work by others demonstrated that BHQ application also blunts
85 cortical spreading depression (CSD) susceptibility in mouse S218L (21). Given these results, a further
86 examination of fruit fly synapses could be valuable for uncovering basic molecular and
87 electrophysiological consequences of $Ca_V2.1$ gains of function.

88 For the present study, we characterized the fruit fly as a way to model neuronal effects of FHM1-
89 causing mutations. We neuronally expressed *cacophony* transgenes harboring the *Drosophila*
90 *melanogaster* equivalents of RQ or SL – or both RQ and SL concurrently (denoted as "DM" for "double
91 mutant"). On the organismal level, neuronal expression of SL or DM transgenes drastically impaired
92 overall health. Not surprisingly, SL and DM transgenes also markedly enhanced aspects of evoked and
93 spontaneous neurotransmission, consistent with prior studies in mice. Through a combination of
94 genetics, RNA interference, pharmacology, and electrophysiology, we uncovered evidence that a
95 canonical intracellular Ca^{2+} signaling pathway influences levels of neurotransmission and
96 hyperexcitability in the context of gain-of-function Drosophila Ca_V2.

97

98 **RESULTS**

99 **Transgenic Drosophila Ca_V2 "FHM1" channels cause coarse larval phenotypes and fly lethality**

100 We undertook a reverse-translational approach in *Drosophila melanogaster* to study the impact
101 that FHM1-inducing $Ca_V2.1$ amino-acid substitutions may exert on the level of individual synapses.
102 Drosophila *cacophony* encodes the $\alpha1$ subunit of all fruit fly Ca_V2-type channels. We cloned two amino-

103 acid substitutions that cause human FHM1 (S218L and R192Q) into the analogous codons of a
104 functional Drosophila *UAS-cacophony (cac)-eGFP* transgene (22). Single mutant transgenes are herein
105 termed "SL" (*UAS-cac-eGFP*^{S161L}) (20) or "RQ" (*UAS-cac-eGFP*^{R135Q}) (Fig. 1A). We also generated a
106 double mutant transgene containing both mutations on the same cDNA clone, termed "DM" (*UAS-cac-*
107 *eGFP*$^{R135Q,\ S161L}$). "WT" signifies previously characterized wild-type *UAS-cac-eGFP*^{WT} transgenes (22).

108 We expressed WT, DM, SL, and RQ *UAS-cac-eGFP* transgenes in post-mitotic Drosophila
109 neurons using the *elaV(C155)-Gal4* driver and the *Gal4/UAS* expression system (23, 24). Initially, we
110 examined transgenic animals for visible phenotypes. Neuronal expression of either SL or DM caused
111 larvae to move in a jerky, uncoordinated manner. At the early third instar stage, SL- and DM-expressing
112 animals developed protruding, anterior spiracles prematurely – well before the normal time point of
113 wandering third instar stage and pupation (Fig 1B). Our initial observations also indicated that SL- and
114 DM-expressing animals were not present in expected Mendelian proportions, so we decided to quantify
115 this potential viability phenotype.

116 We quantified viability of transgenic animals by setting up test crosses and counting adult
117 progeny. For each transgene (WT, DM, SL, and RQ), we set up test crosses (*elaV(C155)-Gal4* females x
118 *Balancer Chromosome*/*UAS-cac-eGFP* males) and counted the number of transgenic *UAS-cac-GFP-*
119 expressing adult progeny and the number of sibling flies carrying a balancer chromosome. We also set
120 up a *Gal4* and balancer chromosome control cross lacking any *UAS-cac-eGFP* transgenes (Table 1).
121 Compared to animals expressing the WT transgene, viability was dramatically diminished for animals
122 expressing the SL and DM transgenes. It was also dramatically diminished for SL- and DM-expressing
123 animals compared to genetically matched siblings carrying the *elaV(C155)-Gal4* driver and a balancer
124 chromosome (Fig. 1C, Table 1). By contrast, WT- and RQ-expressing animals did not show significant
125 defects in viability or statistical differences from the Gal4 control cross. As expected *a priori*, there was a
126 some depressed viability in animals carrying a balancer chromosome. (Fig. 1C, Table 1).

127

128

129

130 **Table 1. Test Crosses and Survival of Adult Progeny.**

elaV(C155)-Gal4* x *Balancer /&	*GAL4/+; &/+* progeny (female)	*GAL4/+; Balancer/+* progeny (female)	Normalized Viability Index for & (female)	*GAL4/Y; &/+* progeny (male)	*GAL4/Y; Balancer/+* progeny (male)	Normalized Viability Index for & (male)
& = +	52 (30.6%)	37 (21.8%)	85.1	53 (31.2%)	28 (16.5%)	114.6
& = *UAS-cac^{WT}-GFP*	190 (30.3%)	115 (18.3%)	100.0	205 (32.6%)	118 (18.8%)	105.2
& = *UAS-cac^{DM}-GFP*	**132 (12.7%)*** **	**499 (48.0%)**	**16.0**	**38 (3.7%)*** ###**	**371 (35.7%)**	**6.2**
& = *UAS-cac^{SL}-GFP*	**38 (12.3%)*** **	**136 (44.2%)**	**16.9**	**17 (5.5%)*** #**	**117 (38.0%)**	**8.8**
& = *UAS-cac^{RQ}-GFP*	157 (29.0%)	128 (23.6%)	74.2	147 (27.1%)	110 (20.3%)	80.9

131

132 Crosses were performed utilizing *elaV(C155)-Gal4* virgin females x *w/Y; Balancer/ (UAS-*
133 *cac-GFP or +)* males. Male and female progeny were counted separately. As expected for
134 fruit fly balancer chromosomes, there was lethality associated with inheriting a balancer
135 chromosome. Separately, there was profound lethality associated with inheriting either the
136 *UAS-cac^{DM}-GFP* or *UAS-cac^{SL}-GFP* transgenes driven by pan-neuronal *elaV(C155)-Gal4*.
137 & - denotes the chromosome utilized opposite the balancer in males in the test cross.
138 Normalized Viability Index scores were all calculated starting with the non-Balancer :
139 Balancer progeny ratio; this value was then normalized against the female progeny ratio
140 for the cross where & = *UAS-cac^{WT}-GFP* – i.e., 190/115 = a normalized baseline value of
141 100.0. For statistical analyses, raw progeny counts were used. *** $p < 0.001$ by Fisher's
142 exact test, compared to gender-matched progeny counts, utilizing the *UAS-cac^{WT}-GFP* as
143 the control. ### $p < 0.001$, # $p = 0.05$, comparing DM- and SL- expressing males vs. DM-
144 and SL-expressing females respectively.

145 Sex or gene dose of the SL and DM transgenes could influence viability. In Drosophila, X-linked
146 dosage compensation equalizes the expression of X-linked genes by doubling X-linked gene
147 transcription in males (25-27). The X-linked neuronal enhancer trap Gal4 line *elaV(C155)-Gal4* should be
148 expressed at higher levels in hemizygous *elaV(C155)-Gal4/Y* males than in heterozygous *elaV(C155)-*
149 *Gal4*/+ females. Thus, effects of driving *UAS* transgenes could be stronger in males. Counting male vs.
150 female progeny of SL- and DM-expressing flies revealed that while viability was starkly diminished for
151 both sexes, it was also significantly lower in SL- and DM-expressing males than in SL- and DM-
152 expressing females (Fig. 1C, Table 1).

153 Finally, we assessed adult fly longevity, comparing WT and DM transgenic flies (Figs. 1D, E). For
154 females, transgenic WT (mean survival: 63 days, n = 23) and driver control *elaV(C155)-Gal4/+* animals
155 (66 days, n = 16) did not differ with respect to survival. Transgenic DM females (22.5 days, n = 28) had
156 severely stunted longevity (Fig. 1D; $p < 0.0001$, Log-rank test). The results for males were consistent:
157 longevity of transgenic WT males (median survival: 56 days, n = 38) and driver control *elaV(C155)-*
158 *Gal4/Y* animals (54.5 days, n = 22) did not differ statistically. By contrast, the survival of transgenic DM
159 males (14.5 days, n = 10) was markedly diminished (Fig. 1E; $p < 0.0001$, Log-rank test).
160

161 **Cac-GFP expression levels are comparable across transgenic constructs and Cac-GFP localizes**
162 **to synaptic active zones**

163 We investigated why SL- and DM-expressing animals were showing diminished viability. We
164 considered the possibility that excessive quantities of α1 protein generated via the *GAL4/UAS*
165 expression system could reduce viability. However, prior studies showed that neuronal overexpression of
166 the WT *UAS-cac-eGFP* transgene renders no discernible structural, behavioral, or electrophysiological
167 abnormalities. Additionally, overexpressed Cac-GFP protein efficiently localizes to active zone structures
168 at synapses like the larval neuromuscular junction (NMJ) (20, 22, 28-31).

169 We assessed whether differential expression or localization of each *UAS-cac-eGFP* could
170 underlie observed reductions in viability. Using wandering third instar larvae, we quantified and
171 compared levels of *elaV(C155)-Gal4*-driven transgene expression for transgenic lines: WT (published
172 line - *UAS-cac-eGFP*^{786c}) (22), RQ (*UAS-cac-eGFP*$^{R/Q(1M)}$) (this study), SL (*UAS-cac-eGFP*$^{S/L(3-2M)}$) (20),
173 and DM (*UAS-cac-eGFP*$^{DM(2M)}$) (this study). We used an anti-GFP antibody to detect Cac-GFP and co-
174 stained with a monoclonal antibody against the presynaptic ELKS/CAST active zone protein Bruchpilot
175 (Brp) (32) in the central nervous system and synaptic structures. We then quantified Cac-GFP staining
176 levels and intensity by immunofluorescence microscopy. In the central nervous system, we found no
177 significant differences in Cac-GFP protein intensity regardless of genotype or transgene insertion (Figs.
178 2A-E, Red channel). We next considered Cac-GFP localization at the NMJ. We found that all WT and
179 mutant transgenic Cac-GFP proteins successfully localized to synaptic active zones as previously

180 reported for the original WT constructs (22, 28). By co-staining with anti-Brp and anti-GFP, we observed
181 significant Cac-GFP protein at Brp-positive NMJ active zones for all chosen transgenic lines (Fig. 2F-I).
182

183 **DM-expressing NMJs show small changes in bouton number and glutamate receptor density**

184 Transgenic mutant Cac-GFP expression could potentially affect synapse growth or development.
185 We previously found no abnormalities in NMJ synaptic growth for SL-expressing flies (20). For this study,
186 we extended our analysis for the DM transgene line by co-staining third instar larval NMJs with
187 antibodies against the Drosophila PSD-95 homolog, Discs Large (Dlg) and the GluRIIA glutamate
188 receptor subunit. We observed a small numerical decrease in the number of Dlg-positive synaptic
189 boutons at DM-expressing NMJs compared to control WT-expressing NMJs. This small decrease was
190 statistically significant only for segment A2, muscle 6/7 (Fig. 2J). Additionally, we found no significant
191 change in the number of glutamate receptor clusters per NMJ comparing WT-expressing synapses and
192 DM-expressing synapses (Fig. 2K).

193 At DM-expressing NMJs, the percentage of the synaptic area covered by the GluRIIA clusters –
194 normalized to total Dlg area – was slightly but significantly increased (Fig. 2L). Moreover, we also
195 observed a very small (~ 7%), but statistically significant increase in the average intensity of GluRIIA-
196 containing glutamate receptor clusters, normalized to Dlg intensity (Fig. 2M) – while average Dlg intensity
197 itself was unchanged between WT- and DM-expressing NMJs. In principle, an expansion of the synaptic
198 area capable of receiving neurotransmitter and a slightly denser packing of GluRIIA-containing receptors
199 could yield gains in synaptic transmission (33). However, the magnitude of any such change based on
200 this postsynaptic staining profile alone (< 10% increase in receptor density) would likely be small or
201 nonexistent. We elected to conduct finer analyses by electrophysiology.
202

203 **DM-, SL- and RQ-expressing NMJs display hyperexcitable evoked synaptic discharges**

204 Coarse phenotypes from neuronally expressed DM and SL transgenes (Fig. 1) suggested
205 abnormal neuronal or synapse function. We turned to NMJ electrophysiology to document possible
206 synaptic dysfunctions caused by the mutant transgenes. We hypothesized that the neuronal expression

207 of gain-of-function *UAS-cac-GFP* transgenes could result in enhanced evoked NMJ neurotransmission in
208 Drosophila, similar to the knock-in mouse FHM1 models.

209 Expression of both SL and DM significantly increased EPSP amplitudes across a range of low
210 extracellular [Ca^{2+}] (0.2–0.5 mM) (Fig. 3A, 3D; data for 0.4 mM $[Ca^{2+}]_e$ are shown) (20). Expression of
211 RQ also increased average NMJ EPSP amplitudes, but this increase was not statistically significant (Fig.
212 3A). Interestingly, neither calculated quantal content (QC) (Fig. 3B) nor calcium cooperativity of release
213 for mutant lines were significantly different than WT across this range of 0.2–0.5 mM [Ca^{2+}] (Fig. 3C) (20)
214 (but see more detailed quantal analyses later).

215 In the course of collecting evoked neurotransmission data, we noted that the EPSP waveforms of
216 RQ, SL, and DM animals were sometimes abnormal (compare Figs 3D, E). Specifically, we observed two
217 distinct phenotypes: 1) 'extra discharges' ("ED"), in which supernumerary spiking events occurred during
218 the decay phase of the EPSP waveform (Fig. 3E, left); and 2) 'shoulders,' in which there was an
219 extended discharge during the decay phase of the EPSP (Fig. 3E, right), causing a discontinuity in the
220 decay. These phenotypes were somewhat reminiscent of a broadening of the end-plate potential
221 previously reported at the NMJs of SL knock-in mice (11). The SL-expressing NMJs produced only the
222 extra discharge type of abnormal waveform, whereas the RQ-expressing NMJs produced only the
223 shoulder form (Figs. 3E, F). Consistent with both mutations being present in DM, those NMJs exhibited
224 both types of abnormal waveform (Fig. 3F). Finally, we generated "RQ only" animals – null cac^{HC129}
225 mutant larvae rescued to viability by expression of the RQ transgene (we were unable to generate similar
226 "SL only" or "DM only" animals, likely due to deleterious gains of function from the SL mutation). In the
227 case of "RQ only", the waveform dysfunction closely matched that shown by the RQ-expressing NMJs
228 (Fig. 3F) – i.e. a shoulder waveform phenotype was present.

229 Next, for the SL- and DM-expressing animals, we assessed the severity of the extra discharge
230 phenotype by counting the number of extra discharge events per 30 evoked pulses (30 recording
231 sweeps at 1 Hz per NMJ). Quantification confirmed that SL- and DM-expressing NMJs were highly
232 dysfunctional, possibly due to underlying neuronal hyperexcitability (Fig. 3G). A previous study in
233 Drosophila demonstrated that magnesium in the recording saline can mask defects in the excitability of

234 neurons (34). Therefore, we extended our analyses by conducting additional WT and DM recordings in
235 saline with lowered $MgCl_2$ (6 mM vs. 10 mM for normal saline). DM-expressing NMJs displayed extreme
236 dysfunction in 6 mM $MgCl_2$, both in terms of the percentage of NMJs that produced supernumerary
237 discharges (100%, Fig. 3H) and the number of extra discharges counted per 30 presynaptic pulses (Fig.
238 3I). By contrast, WT-expressing NMJs showed no significant dysfunction (Figs. 3H, I). In all, SL- and DM-
239 expressing NMJs displayed evoked gain-of-function phenotypes consistent with prior mammalian FHM1
240 mutant analyses.
241

242 **SL- and DM-expressing NMJs show enhanced spontaneous miniature EPSPs with respect to both**
243 **amplitude and frequency**

244 The evoked neurotransmission data indicated synapse hyperexcitability in the mutant transgenic
245 flies. Mammalian models of FHM1 also show dysfunctional spontaneous neurotransmission (10, 11).
246 Therefore, we extended our electrophysiological analyses to quantal neurotransmission. We observed a
247 striking phenotype: for SL- and DM-expressing NMJs, there was a significant enhancement in both
248 amplitude and frequency of spontaneous miniature EPSPs (mEPSPs) (Figs. 4A-C, Table 2). By contrast,
249 neither an increase in spontaneous mEPSP amplitude nor mEPSP frequency were observed for RQ- or
250 WT-expressing NMJs compared to non-transgenic w^{1118} controls (Figs. 4B-E, Table 2). Interestingly, we
251 also noted that the spontaneous events at SL- and DM-expressing NMJs also included a small minority
252 of gigantic spontaneous events (10-40 mV) that were never seen in controls or RQ-expressing NMJs
253 (Figs. 4A, D, E). These gigantic events were seen in the complete absence of presynaptic nerve
254 stimulation in nerves that had already been severed from the central nervous system. Follow-up
255 analyses of thousands of individual spontaneous events per genotype revealed that increases in
256 spontaneous amplitudes were due to an overall increase in the size distribution of the events at SL- and
257 DM-expressing NMJs (Figs. 4D, E), which also included the rare gigantic events, never observed at
258 w^{1118}, WT-, or RQ-expressing NMJs (Fig. 4D).

259 **Table 2. Raw electrophysiological data of spontaneous (mEPSP) events – Ca^{2+} and Na_V.**

Line	Saline	n	Average mEPSP (mV)	mEPSP Freq (Hz)	Median mEPSP (mV)	Maximum mEPSP (mV)	Resting Membrane V (mV)	Analysis Figures
w^{1118}	0.5 mM [Ca^{2+}]	13	0.86 ± 0.07	4.6 ± 0.4	0.69	11.53	-62.9 ± 0.9	4, 5
GAL4 > WT		17	0.77 ± 0.05	2.8 ± 0.2	0.67	7.24	-67.8 ± 0.9	4, 5, 6
GAL4 > DM		25	1.75 ± 0.22	5.8 ± 0.7	1.04	36.91	-68.2 ± 1.2	4, 5, 6
GAL4 > SL		12	1.32 ± 0.16	6.7 ± 1.0	0.76	44.42	-65.4 ± 0.9	4, 5, 6
GAL4 > RQ		13	0.77 ± 0.05	3.4 ± 0.4	0.61	3.88	-64.7 ± 1.0	4, 5
w^{1118}	0.4 mM [Ca^{2+}]	15	0.70 ± 0.03	3.7 ± 0.2	0.61	3.37	-61.4 ± 0.4	3
GAL4 > WT		25	0.79 ± 0.05	3.1 ± 0.2	0.66	5.41	-64.2 ± 0.9	3
GAL4 > DM		17	1.48 ± 0.13	6.0 ± 0.7	1.10	41.17	-62.2 ± 0.6	3
GAL4 > SL		14	1.66 ± 0.19	6.6 ± 1.1	1.18	57.90	-65.1 ± 1.6	3
GAL4 > RQ		12	0.79 ± 0.06	4.3 ± 0.4	0.69	3.38	-66.5 ± 1.7	3
w^{1118}	0.2 mM [Ca^{2+}]	9	0.64 ± 0.03	3.9 ± 0.3	0.56	2.73	-61.2 ± 0.9	5
GAL4 > WT		12	0.70 ± 0.06	2.5 ± 0.3	0.59	2.88	-67.1 ± 1.3	5
GAL4 > DM		19	1.34 ± 0.08	5.2 ± 0.6	1.11	19.95	-61.8 ± 0.9	5
GAL4 > SL		14	0.94 ± 0.08	7.0 ± 1.1	0.77	5.93	-65.6 ± 1.6	5
GAL4 > RQ		8	0.77 ± 0.04	2.0 ± 0.4	0.66	2.88	-58.7 ± 0.5	5
GAL4 > WT	0 mM [Ca^{2+}]	9	0.73 ± 0.05	2.7 ± 0.3	0.61	3.31	-60.1 ± 1.4	5
GAL4 > DM		10	1.15 ± 0.09	8.4 ± 1.6	0.98	6.59	-58.0 ± 1.6	5
GAL4 > SL		11	1.17 ± 0.11	12.6 ± 2.3	0.93	5.42	-58.7 ± 0.6	5
GAL4 > WT	BAPTA-AM and TTX controls	18	0.73 ± 0.02	4.2 ± 0.4	0.65	3.04	-66.5 ± 1.2	5
GAL4 > DM		16	1.29 ± 0.14	7.4 ± 0.7	0.92	41.56	-64.4 ± 0.8	5
GAL4 > WT	+ 10 μM BAPTA-AM	9	0.62 ± 0.06	1.6 ± 0.2	0.51	3.67	-60.4 ± 1.9	5
GAL4 > DM		8	1.16 ± 0.10	2.0 ± 0.2	0.97	5.50	-59.5 ± 1.0	5
GAL4 > WT	+ 3 μM TTX	7	0.66 ± 0.05	3.8 ± 0.4	0.54	2.82	-62.1 ± 1.1	5
GAL4 > DM		18	1.09 ± 0.07	6.9 ± 0.7	0.85	9.82	-62.5 ± 0.7	5

Average mEPSP amplitudes ± SEM and mEPSP frequencies ± SEM for selected conditions. Also given: median mEPSP amplitudes and maximum mEPSP amplitudes achieved for spontaneous events analyzed (~100 per NMJ). *w^{1118}* is a non-transgenic wild-type control. WT, DM, SL, and RQ are shorthand for the indicated *UAS-cac-eGFP* transgene being driven in male progeny presynaptically by the *elaV(C155)-GAL4* driver. These data illustrate differential effects when lowering extracellular [Ca^{2+}], chelating Ca^{2+} with BAPTA-AM, or inactivating Na_V channels with TTX.

We checked if acute *cac* transgene expression was sufficient to cause spontaneous neurotransmission phenotypes. We utilized the temperature-sensitive *$Gal80^{TS}$/TARGET* system to temporally control expression of the DM transgene (35). To conduct this experiment, we generated *elaV(C155)-Gal4 >> UAS-cac^{DM}* animals with a ubiquitous *$Gal80^{TS}$* transgene (35). $Gal80^{TS}$ protein halts

272 Gal4-induced gene expression at permissive temperatures (25ºC) but not at restrictive temperatures
273 (29ºC). For our experiment, animals raised at 25ºC throughout life had no discernible spontaneous
274 neurotransmission hyperexcitability (Fig. 4F). By contrast, animals started at 25ºC and shifted to 29ºC for
275 the final 24 or 48 hours before third instar NMJ recording showed progressively more spontaneous
276 hyperexcitability (Figs. 4F, G).
277
278 **Gigantic spontaneous events require extracellular calcium and sodium channel activity**
279 Prior work proposed that mammalian neuronal dysfunction downstream of FHM1 mutations may
280 be calcium-dependent (12). We tested whether the observed effects on quantal size in our model could
281 be calcium-dependent. First, we reduced the extracellular [Ca^{2+}] in the recording saline from 0.5 mM to
282 0.2 mM. Consistent with classic characterizations of Drosophila NMJ properties (36), low calcium did little
283 to change the distribution of mEPSP size, the median mEPSP size, or the 25th-75th percentiles of
284 mEPSP size – all of which remained normal for WT and elevated for SL- and DM-expressing NMJs
285 (Figs. 5A, B, Table 2). However, lowering extracellular [Ca^{2+}] almost completely abrogated gigantic (10-
286 40 mV) spontaneous events at SL- and DM-expressing NMJs – and it completely eliminated the very
287 largest ones (Figs. 5A, B). This suggested that these gigantic events somehow relied on a sufficient
288 driving force of presynaptic calcium influx – and potentially on spontaneous presynaptic nerve firing.
289 We extended these analyses by altering the recording saline in three additional ways: 1) zero
290 extracellular calcium; 2) adding the membrane-permeable calcium chelator, 1,2-Bis (2-aminophenoxy)
291 ethane-N,N,N′,N′-tetra acetic acid tetrakis (acetoxymethyl ester) (BAPTA-AM, 10 μM); or 3) adding
292 tetrodotoxin (TTX, 3 μM) to block voltage-gated sodium channels. We compared WT-expressing and
293 DM-expressing NMJs (and SL-expressing NMJs in the case of zero calcium). All three manipulations
294 produced a similar effect on mEPSP size for the gain-of-function mutants: an elimination of gigantic
295 spontaneous events, but a persistence of overall elevated mEPSP size (Figs. 5C-F, Table 2). By
296 contrast, these manipulations had minimal to no effect on the distribution of mEPSP amplitudes at WT-
297 expressing NMJs (Figs. 5C-D, Table 2).
298

299 **Large spontaneous events are due to multi-vesicular release**

300 The presence of gigantic spontaneous mEPSPs that were sensitive to low calcium, calcium
301 chelation, and TTX treatment suggested the possibility of spontaneous multi-vesicular release at SL- and
302 DM-expressing NMJs. If this were true, traditional analysis of spontaneous mEPSPs would result in an
303 overestimation of average quantal size (Fig. 4B) and underestimation of average QC (Fig. 3B) for SL-
304 and DM-expressing NMJs.

305 We utilized the method of failures to better resolve questions about quantal size and QC. At very
306 low concentrations of extracellular calcium, synapses like the NMJ are essentially limited to a one-or-
307 none evoked response in which stimulation of the presynaptic nerve either leads to the release of a
308 single vesicle or fails to release any vesicles (37). By conducting failure analyses, it is possible to
309 measure the distribution of quantal events and also to estimate QC in a way that eliminates confounds of
310 higher concentrations of calcium. First, we conducted failure analysis recordings at 0.14 mM $[Ca^{2+}]_e$ for
311 WT-, DM-, and SL-expressing NMJs (Figs. 6A-C). For this condition, the evoked events for SL- and DM-
312 expressing NMJs were far larger on average than those observed WT-expressing NMJs (Fig. 6C –
313 EPSP). This was due to a large proportion of events of > 2 mV for the SL- and DM-expressing conditions
314 (compare Figs. 6A, B for WT vs. DM). Furthermore, even in this low level of extracellular Ca^{2+}, many of
315 DM and SL events represented multi-vesicular release rather than the release of a single large vesicle.
316 We calculated values of QC of > 2 for both mutant conditions at 0.14 mM $[Ca^{2+}]_e$ (QC = m = ln[(# trials)/(#
317 failures)] (38)) (Fig. 6C).

318 To test if lower calcium could generate a leftward shift in event size, we applied a more restrictive
319 condition of 0.1 mM $[Ca^{2+}]_e$ to DM-expressing NMJs. At 0.1 mM $[Ca^{2+}]_e$ the proportion of failures was very
320 high for DM-expressing NMJs, with events over 4 mV all but absent, and events greater than 1.5 mV also
321 less prevalent (Fig. 6C). The first peak in the distribution of events, which is reflective of single vesicle
322 size (38), was centered near 0.7 mV, a value consistent with single-vesicle responses of normal size for
323 the Drosophila NMJ (36). Together, these data suggested that the observed large events at SL- and DM-
324 expressing NMJs – regardless of whether spontaneous or failure analysis-evoked – were likely due to
325 multi-vesicular release (see Fig. 6E, spontaneous and failure analyses distributions side-by-side).

326

327 **PLCβ loss genetically suppresses spontaneous excitability**

328 For SL- and DM-expressing NMJs, we hypothesized that specific cellular cues could dictate the
329 various electrophysiological phenotypes we documented: multi-vesicular quantal events, gigantic TTX-
330 sensitive spontaneous events, and enhanced NMJ excitability. We inquired as to what the molecular
331 nature of those cues might be. Our experiments indicated that intracellular calcium or intracellular
332 calcium signaling processes might be important (Fig. 5). Additionally, recent data from the mouse calyx
333 of Held demonstrated that S218L knock-in synapses have enhanced resting intracellular calcium (12).
334 We hypothesized that altered intracellular calcium signaling or handling could impact myriad intracellular
335 signals and investigated which signaling pathways might be relevant.

336 This line of inquiry spurred a directed genetic approach examining regulators of intracellular
337 calcium release to test if inhibition of any of these factors may influence gain-of-function Ca_V2
338 phenotypes at the synapse (Fig. 7A). We sought to identify suppressors capable of reversing gains of
339 Ca_V2 function caused by the SL and DM transgenes.

340 Prior studies of Drosophila NMJ presynaptic homeostatic potentiation – which involves the
341 potentiation of Ca_V2 – suggested some possible candidate molecules (39, 40). Additionally, we
342 previously showed that the Drosophila PLCβ homolog *phospholipase-C at 21C* (*Plc21C*) is necessary for
343 the neuronal homeostatic potentiation mechanism (41). Plc21C is one of two Drosophila Phospholipase-
344 Cβ (PLCβ) family members, and is expressed in the nervous system (42). Canonically, PLCβ proteins
345 cleave phosphatidylinositol 4,5-bisphosphate (PIP_2) to generate soluble inositol triphosphate (IP_3), as
346 well as membrane-bound diacylglycerol (DAG). These signaling factors influence synaptic transmission
347 in a variety of ways, including direct modulation of Ca_V2 (43), and they have been shown to act at several
348 synapses, including the NMJ (44-49).

349 We targeted *Plc21C* gene expression in neurons with a previously verified *UAS-Plc21C(RNAi)*
350 construct, $Plc21C^{GD11359}$ (41, 50). Compared to the NMJs of w^{1118} and WT controls, those in which only
351 *Plc21C* had been knocked down presynaptically exhibited no discernable baseline changes in mEPSP
352 size (Fig. 7B, Table 3) – or as previously documented, EPSP size, or QC (41). By contrast, in DM-

353 expressing NMJs such *Plc21C* knockdown alleviated aspects of NMJ hyperexcitability. Specifically, there

354 was a leftward shift in the distribution of spontaneous events (Fig. 7B, Table 3).

355

356 **Table 3. Raw electrophysiological data of spontaneous (mEPSP) events – impairment of**
357 **intracellular Ca^{2+} handling pathway.**

Line	Experiment (all 0.5 mM Ca^{2+})	n	Average mEPSP (mV)	mEPSP Freq (Hz)	Median mEPSP (mV)	Maximum mEPSP (mV)	Resting Membrane V (mV)	Analysis Figures
w^{1118} females	*Plc21C* RNAi baseline	27	0.81 ± 0.05	4.3 ± 0.3	0.64	7.16	-62.2 ± 0.6	7
Plc21C(RNAi) males		12	0.80 ± 0.06	2.0 ± 0.2	0.61	4.50	-66.5 ± 0.9	N/A
Plc21C(RNAi) females		6	0.83 ± 0.02	3.8 ± 0.9	0.59	7.68	-61.6 ± 0.3	7
GAL4 > DM females	suppression of DM	19	1.28 ± 0.08	5.8 ± 0.5	1.01	7.62	-67.0 ± 1.2	7
GAL4 > DM + Plc21C(RNAi) females		13	0.78 ± 0.04	5.2 ± 0.6	0.68	3.89	-64.9 ± 1.6	7
GAL4; $itpr^{ug3}$/+	suppression of *DM*	9	0.74 ± 0.04	3.7 ± 0.2	0.64	3.34	-61.3 ± 0.6	7
GAL4 > DM; $itpr^{ug3}$/+		14	1.05 ± 0.06	6.1 ± 0.5	0.86	16.21	-65.8 ± 0.7	7
GAL4; RyR^{E4340K}/+	suppression of *DM*	13	0.83 ± 0.03	3.3 ± 0.3	0.70	3.38	-63.0 ± 0.5	7
GAL4 > DM; RyR^{E4340K}/+		17	0.91 ± 0.04	5.1 ± 0.8	0.76	5.13	-62.5 ± 0.9	7
GAL4 > WT	XestC and LiCl controls	19	0.80 ± 0.02	2.3 ± 0.3	0.71	2.59	-69.6 ± 1.1	8
GAL4 > DM		30	1.63 ± 0.13	6.6 ± 0.7	1.08	51.03	-65.8 ± 0.7	8
GAL4 > WT	+ 5 μM XestC	7	1.04 ± 0.04	3.5 ± 0.9	0.78	3.80	-69.8 ± 2.2	8
GAL4 > DM		14	1.14 ± 0.11	6.4 ± 1.1	0.81	30.76	-67.2 ± 1.3	8
GAL4 > WT	+ 10 mM LiCl	11	0.81 ± 0.03	3.2 ± 0.4	0.73	4.09	-66.6 ± 1.3	8
GAL4 > DM		12	1.2 ± 0.06	4.1 ± 0.4	0.98	6.34	-68.8 ± 1.7	8

358

359 Average mEPSP amplitudes ± SEM and mEPSP frequencies ± SEM for selected
360 experimental conditions. Also given are the median mEPSP amplitude and the maximum
361 mEPSP amplitudes achieved for all spontaneous events analyzed per genotype (~100 per

362 NMJ). w^{1118} is a non-transgenic wild-type control. WT and DM are shorthand for the
363 indicated *UAS-cac-eGFP* transgene being driven in progeny presynaptically by the
364 *elaV(C155)-GAL4* driver. This table illustrates differential effects when impairing an
365 intracellular calcium handling pathway through mutation of the *Plc21C*, *itpr*, and *RyR*
366 genes, or through pharmacological application of Xestospongin C or LiCl.

367

368 **IP_3R and RyR point mutations strongly suppress hyperexcitability**

369 We hypothesized that Plc21C could exert effects on spontaneous neurotransmission via one of
370 several components of its canonical signaling pathway (e.g. PIP_2, DAG, or IP_3). Notably, IP_3 acts through
371 the IP_3 receptor (IP_3R), an intracellular calcium channel located on the endoplasmic reticulum (ER). At
372 other model synapses, release of Ca^{2+} from the intracellular stores can promote the release of
373 neurotransmitter-laden vesicles and contribute to the amplitudes of spontaneous events (51-54).
374 Moreover, IP_3R has been proposed to play a role in spontaneous vesicle release through calcium-
375 induced calcium release (CICR) (55), and increased ER Ca^{2+} release was recently shown to potentiate
376 synaptic transmission at the Drosophila NMJ (56).

377 We examined the Drosophila IP_3R gene (*itpr*). Homozygous *itpr* mutations are lethal, so we first
378 tested a heterozygous loss-of-function condition. Since IP_3R clusters consist of multiple units, we
379 hypothesized that we might be able to disrupt them through a loss-of-function point mutation, $itpr^{\mu g3}$, a
380 mutant possessing a missense mutation in the IP_3R ligand-binding domain (57). $itpr^{\mu g3}$/+ phenocopied
381 *Plc21C* knockdown at DM-expressing NMJs: the mEPSP amplitude was partially reduced toward WT
382 levels, and the number of giant, spontaneous events was diminished (Figs. 7C, D, Table 3). Importantly,
383 on its own $itpr^{\mu g3}$/+ did not significantly affect the baseline amplitude or distribution of mEPSPs (Fig. 7C,
384 Table 3).

385 We performed analogous experiments with a Drosophila ryanodine receptor gene (*RyR*)
386 mutation. Tetrameric RyR channels have been reported to contribute to CICR downstream of IP_3Rs (55).
387 Additionally, gigantic spontaneous miniature potentials at other model synapses are mediated by RyR
388 and rapid expulsion of calcium from presynaptic stores (58-62). We found that the heterozygous *RyR*
389 point mutant RyR^{E4340K}/+ (63) almost completely suppressed the DM mEPSP phenotype. The increased
390 average mEPSP in the DM-expressing background was suppressed (Figs. 7C, E, Table 3), and the

391 gigantic spontaneous events were abrogated (Figs. 7C, E, Table 3). Control recordings showed that
392 *RyR*^{E4340K}/+ did not affect the baseline amplitude or distribution of mEPSPs (Fig. 7C).

393 Because the *RyR*^{E4340K}/+ background provided such a strong suppression of spontaneous
394 mEPSP hyperexcitability at DM-expressing NMJs, we checked if it could also suppress hyperexcitability
395 in the context of evoked excitation. As shown before, when incubated in low extracellular magnesium,
396 100% of the DM-expressing NMJs showed a hyperexcitability dysfunction, with high expressivity of extra,
397 epileptiform discharges (Figs. 3H,I; 7F). By contrast, in a heterozygous *RyR*^{E4340K}/+ genetic background,
398 this hyperexcitability was somewhat suppressed, in terms of both the penetrance of NMJs with extra
399 evoked discharges and the expressivity of the extra discharge dysfunction at individual NMJs (Fig. 7F).

400

401 **Spontaneous mEPSP hyperexcitability can be suppressed pharmacologically**

402 Our data for genetic manipulations affecting Plc21C, IP_3R, and RyR show that it is possible to
403 attenuate DM-induced gain-of-function mEPSP phenotypes by manipulating factors involved in
404 intracellular Ca^{2+} release. In addition to genetic manipulations, we wondered if chronic or acute
405 pharmacological manipulations could also be effective. We turned to two agents to test this idea: lithium
406 (10mM LiCl in larval food) and Xestospongin C (5 μM in recording saline). Chronic exposure to LiCl
407 inhibits inositol monophosphate phosphatase, eventually resulting in a disruption of the recycling process
408 that generates PIP_2 (64, 65). By contrast, Xestospongin C has been characterized as a membrane-
409 permeable inhibitor of IP_3 receptors (66, 67). Either chronically feeding larvae LiCl or applying
410 Xestospongin C to the recording bath caused a significant leftward shift in the overall size distribution of
411 spontaneous amplitudes (Figs. 8A-C), reminiscent of the effects observed for *Plc21C*, *itpr*, and *RyR*
412 losses of function. The acute Xestospongin C application seemed to exert a stronger suppression effect
413 in this regard, while the chronic LiCl application exerted a stronger suppression of the gigantic
414 spontaneous events (Figs. 8 A-C, Table 3). Notably, neither pharmacological manipulation diminished
415 baseline spontaneous neurotransmission in WT-expressing control NMJs (Figs 8A-C, Table 3).

416

417 **DISCUSSION**

418 We generated fruit flies designed to mimic the effects of FHM1-inducing $Ca_V2.1$ channel mutants,
419 R192Q and S218L. Flies expressing the SL and DM transgenes for Drosophila Ca_V2/Cacophony
420 displayed overt phenotypes, including reduced viability (Fig. 1). They also displayed synaptic
421 phenotypes, including enhanced evoked excitability (Fig. 3), stark increases in quantal size and
422 frequency (Fig. 4), giant, spontaneous, sodium channel-dependent events (Figs. 4, 5), and enhanced
423 probability of release at very low calcium (Fig. 6). All of these neurotransmission phenotypes occurred
424 without major alterations to synaptic architecture (Fig. 2). By contrast, RQ-expressing NMJs had only a
425 mild phenotype: EPSP discharges with shoulder-like waveforms (Fig. 3). Genetic knockdown of
426 Drosophila PLCβ or mutations affecting the receptors that gate intracellular calcium stores (IP_3 receptor
427 and Ryanodine receptor) partially alleviated some of the electrophysiological phenotypes (Fig. 7), as did
428 pharmacological manipulations targeting the same processes (Fig. 8). These results suggest that
429 intracellular Ca^{2+} signaling through IP_3 receptors and Ryanodine receptors could influence physiological
430 dysfunction in a gain-of-function Ca_V2 background (Fig. 8D). Additionally, given the ability of TTX to block
431 gigantic spontaneous events – and given our ability to quiet that phenotype through genetic and
432 pharmacological means – impairment of the IP_3 Receptor/Ryanodine Receptor pathway may limit
433 spontaneous neuronal firing by as-yet undetermined mechanisms (Fig. 8D).
434

435 **Similarities between fly mutations and FHM1-causing human mutations**

436 *Evoked Neurotransmission.* Our discovery that SL- and DM-expressing Drosophila NMJs
437 displayed increased evoked excitation, especially at low $[Ca^{2+}]_e$ (Figs. 3, 6) (20), was consistent with
438 findings from diaphragm NMJs in SL knock-in mice (11). In that context, the end-plate potential (EPP)
439 amplitudes were significantly increased at low levels of calcium (0.2 mM), but did not differ from those at
440 wild-type NMJs at physiological calcium (2 mM) (11). Interestingly, at the SL knock-in calyx of Held,
441 excitatory postsynaptic currents (EPSCs) were increased, but this effect was most pronounced at high
442 levels of $[Ca^{2+}]_e$ (12). The extended or epileptiform EPSP discharges caused by expression of the SL-
443 containing transgenic constructs in flies (Fig. 3) were reminiscent of the EPP broadening at SL knock-in
444 NMJs (11). Finally, the severity of the dysfunction in the Drosophila NMJ waveform in the context of

445 decreased extracellular magnesium (6 mM) (Fig. 3) was consistent with a marked increase in calcium
446 current in response to long action potential waveforms in calyces of Held expressing the RQ or SL
447 mutant protein (12, 14).

448 *Enhanced Quantal Frequency.* The enhanced mEPSP frequency at SL- and DM-expressing
449 Drosophila NMJs (Fig. 4, Table 1) was reminiscent of observations in prior FHM1 studies. In the RQ and
450 SL knock-in mice, the NMJs exhibited significant increases in the frequency of mEPPs (9-11).
451 Theoretically, this spontaneous activity could ultimately lead to a buildup of intracellular calcium or a
452 change in intracellular calcium dynamics. In support of this view, at the calyx of Held in SL knock-in mice
453 the frequency of spontaneous mEPSCs was enhanced and resting $[Ca^{2+}]_i$ was elevated (12). In that
454 case, the increase in quantal frequency was partially reversed by adding the cell-permeable calcium
455 chelator EGTA-AM (12).

456 Evidence from several model synapses suggests that Ca_V2 channels can play a prominent role in
457 spontaneous release. In granule cells of the hippocampus, stochastic activity of $Ca_V2.2$-type channels
458 potentiates spontaneous miniature events, and the application of either BAPTA-AM or EGTA-AM is
459 sufficient to inhibit them (68). Other studies demonstrated that P/Q-, N-, and R-type calcium channels
460 also promote spontaneous release (69). Notably, the differences in the spontaneous miniature
461 phenotype between mice harboring the SL and RQ knock-in substitution, or fruit flies expressing
462 mimicking mutations, suggest that the differences in cellular outcomes occur downstream of the Ca_v2
463 channel. This highlights a need for genetic approaches to uncover pathways that might contribute to the
464 divergent phenotypes, as well those that are shared, to better understand the biology downstream of
465 gain-of-function calcium channel activity.

466

467 **Differences between fly mutations and FHM1-causing human mutations**

468 *Quantal amplitudes.* While FHM1 mutations have been shown to enhance spontaneous miniature
469 quantal release frequency in other systems (8-11), there has been no report of increases in spontaneous
470 miniature quantal size due to these mutations. In theory, an increase in the amplitude of mEPSP events
471 at the Drosophila NMJ could be explained by an alteration to the expression and localization of

472 postsynaptic proteins. Yet immunostaining of postsynaptic markers did not strongly support this
473 possibility (Figs. 2J-M), nor did the results of the temperature shift experiments and transient DM
474 expression (Fig. 4G). Instead, failure analyses pointed to alterations to the nature of spontaneous,
475 presynaptic vesicle release (Fig. 6).

476 Why do SL- and DM-expressing NMJs in Drosophila show an increase in quantal size through
477 multi-vesicular release? The synaptic preparation examined is likely to be critical. Evidence from other
478 systems has demonstrated that calcium-channel activity can have a profound effect on quantal size. For
479 example, work at the *C. elegans* NMJ has demonstrated that calcium from intracellular and extracellular
480 sources combines to dictate quantal size and frequency (52). Additionally, spontaneous miniature events
481 with large amplitudes ("maximinis") have been documented at fast inhibitory synapses of the cerebellum
482 (51, 70). Similar to the NMJ activity documented in our study, these maximinis rely on the ability of
483 ryanodine-sensitive stores to support spontaneous calcium transients large enough to cause multi-
484 vesicular release. It is possible that the architecture of a giant synapse like the Drosophila NMJ – which
485 contains hundreds of active zones clustered into individual boutons and has a low level of spontaneous,
486 multi-vesicular release (71) – makes it exquisitely sensitive to small changes in intracellular calcium
487 handling.

488 *Evoked waveforms*. As is the case for the Drosophila NMJ (Fig. 2), the diaphragm NMJ of FHM1
489 knock-in mice displayed EPP broadening (11). The mouse and fly NMJ models are similar in that evoked
490 dysfunction is enhanced by the elicitation of events by stimuli of long duration (14). However, the extra,
491 epileptiform discharges we find at the Drosophila NMJ do not seem to be documented for the
492 mammalian NMJ. An instructive parallel can be drawn between our data and cultures of Drosophila giant
493 neurons, in which manipulation of the voltage-gated potassium current generated altered waveforms,
494 including extra and extended discharges (72, 73). This raises the possibility that some aspects of the
495 FHM1 phenotypes may be caused by the perturbation of other voltage-activated currents, and by
496 synapse excitability more generally (74). This possibility is also consistent with the fact that mutations in
497 the Na^+/K^+ ATPase gene cause pure FHM (75). Given the effectiveness of the Drosophila system for

498 uncovering complex homeostatic relationships amongst ion channel activities, in particular potassium
499 currents, the fly may be a good model for studying the cellular bases of disorders such as FHM1 (76-80).
500

501 **Implications for gain-of-function calcium channel and migraine signaling pathways**

502 One strength of Drosophila is the power of genetic manipulation. In this study, we have shown
503 that the expression of gain-of-function transgenes bearing mutations mimicking those associated with
504 migraine in humans causes overt spontaneous and/or evoked phenotypes. Further, we have shown that
505 impairment of a PLCβ-directed signaling pathway occludes several aspects of spontaneous dysfunction.
506 A simple explanation – but certainly not the only explanation – is that $Ca_V2.1$ gains of function potentiate
507 the activities of the IP_3R and RyR channels (81-84). Our work does not directly show this. However, the
508 implication of PLCβ activity and intracellular calcium handling in hyperexcitability fit with the results of
509 prior migraine studies. One recent RNA profiling analysis of the cerebellum of SL knock-in mice revealed
510 an overrepresentation of several signaling pathway components, including PLCβ (85). Moreover, PLCβ
511 and the release of calcium from intracellular stores have been implicated in signaling by calcitonin gene
512 related peptide (CGRP) (86-88), whose levels are correlated with migraine (89-91). Further investigation
513 will be needed to establish whether there is a causative link between the action of intracellular calcium
514 stores either in inducing migraine or in precipitating neurological events that precede some forms of
515 migraine, like aura and cortical spreading depression.
516

517 **MATERIALS AND METHODS**

518 **Gain-of-function *cacophony* constructs:** To generate *UAS-cac-eGFP*^{SL} transgenes, we used PCR to
519 alter the serine 161 codon to leucine in the pUAST-based *UAS-cac-eGFP* DNA construct (20, 22). This
520 substitution corresponds to S218L in mammalian CACNA1A. To generate *UAS-cac-eGFP*^{RQ} transgenes,
521 we used PCR to change the arginine 135 codon to glutamine. This substitution corresponds to R192Q in
522 mammalian CACNA1A. For the *UAS-cac-eGFP*^{DM} transgene, both mutations were incorporated into the
523 same *UAS-cac-eGFP* construct using PCR to link the overlapping RQ and SL fragments. Transgenic

524 lines were generated by injection of *UAS-cac-eGFP* constructs into a w^{1118} background (The Best Gene,
525 Chino Hills, CA) and mapped and backcrossed.

526 **Drosophila Stocks, Genetics, and Husbandry:** Animals used for viability counts and electrophysiology
527 were generated by driving neuronal expression of *UAS-cac-eGFP* transgenes with *elaV(C155)-GAL4*
528 (23). Multiple *UAS-cac-eGFP* transgenic lines were initially examined to control for possible differences
529 caused by independent *UAS* genomic insertions: WT: *UAS-cac-eGFP*^{786c} (22), *UAS-cac-eGFP*^{422a} (22);
530 SL: *UAS-cac-eGFP*$^{S/L(3\text{-}2M)}$, *UAS-cac-eGFP*$^{S/L(3\text{-}6M)}$, *UAS-cac-eGFP*$^{S/L(3\text{-}8M)}$; RQ: *UAS-cac-eGFP*$^{R/Q(1M)}$,
531 *UAS-cac-eGFP*$^{R/Q(2\text{-}4M)}$; DM: *UAS-cac-eGFP*$^{DM(1M)}$, *UAS-cac-eGFP*$^{DM(2M)}$. After verifying similar expression
532 levels for individual transgenic lines, those lines were used.

533 w^{1118} (92) was used as a non-transgenic wild-type control. The *itpr*^{ug3} (93) and *RyR*^{E4340K} (63)
534 mutant Drosophila stocks were obtained from the Bloomington Drosophila Stock Center (BDSC,
535 Bloomington, Indiana). The *UAS-Plc21C(RNAi)* transformant lines 26557 and 26558 (*Plc21C*^{GD11359}) (94)
536 were obtained from the Vienna Drosophila Resource Center (VDRC, Vienna, Austria). A *Gal80*^{TS}
537 expression line (35) was employed for a temporal Gal4 expression experiment. Flies were raised at 25°C
538 (or 29°C for one temperature shift experiment) in humidity- and light-controlled Percival incubators
539 (Geneva Scientific, Fontana, WI), in glass vials on a standard Drosophila food containing water, agar,
540 molasses, yellow cornmeal, and yeast.

541 **Electrophysiology and Analysis:** Wandering third-instar larvae were selected for analysis. Larvae were
542 dissected in a modified HL3 saline with the following components (and concentrations): NaCl (70 mM),
543 KCl (5 mM), $MgCl_2$ (10 mM or 6 mM as noted), $NaHCO_3$ (10 mM), sucrose (115 mM = 3.9%), trehalose
544 (4.2 mM = 0.16%), HEPES (5.0 mM = 0.12%), and $CaCl_2$ (0.5 mM, unless otherwise noted).
545 Pharmacological agents tetrodotoxin (TTX, Tocris/R&D Systems), BAPTA-AM (Sigma), Xestospongin C
546 (Tocris/R&D), or lithium chloride (LiCl, Sigma) were added as noted for some experiments. For the
547 experiment using TTX (select agent toxin), all appropriate federal regulations and protocols established
548 for the Select Agent Program established by the Centers for Disease Control and Prevention (CDC) and
549 the US Department of Agriculture (USDA) were followed.

550 Electrophysiological data were collected using Axopatch 200B or Axoclamp 900A amplifiers
551 (Molecular Devices, Sunnyvale, CA). Sharp electrode (> 10 MΩ) recordings were taken from muscle 6 of
552 abdominal segments 2 and 3, as described previously (29, 30, 95). Prior to muscle V_m measurements,
553 the Axoclamp 900A was bridge balanced. For the Axopatch 200B, the amplifier was placed in bridge
554 mode (using I-CLAMP FAST for sharp electrode recordings). Before recording from each muscle,
555 electrode resistance was measured and properly compensated by applying a step input and adjusting
556 series resistance. Muscles with a V_m more hyperpolarized than -60 mV and an input resistance of greater
557 than 5 MΩ were deemed suitable for recording (29). Data were digitized using a Digidata 1440A data
558 acquisition system (Molecular Devices), and recorded using the pCLAMP 10 acquisition software
559 (Molecular Devices). For presynaptic nerve stimulation, a Master-8 pulse stimulator (A.M.P. Instruments,
560 Jerusalem, Israel) and an ISO-Flex isolation unit (A.M.P. Instruments) were utilized to deliver
561 suprathreshold stimuli (1 ms unless otherwise indicated) to the appropriate segmental nerve. For each
562 NMJ, the average amplitude of spontaneous miniature excitatory postsynaptic potential EPSPs
563 (mEPSPs) was quantified by measuring approximately 100-200 individual spontaneous release events
564 per NMJ. The average per-NMJ mEPSP amplitudes were then averaged for each genotype. Evoked
565 EPSP amplitude was calculated for each NMJ as the average of 30 events (1 Hz). Quantal content (QC)
566 was determined in two different ways. At low extracellular [Ca^{2+}], QC was calculated by the method of
567 failures, as $m = \ln[(\#\text{ trials})/(\#\text{ failures})]$, as described elsewhere (38). At high extracellular [Ca^{2+}], QC was
568 calculated by dividing EPSP/mEPSP, as described in the text. For analyses conducted across different
569 calcium concentrations, QC was corrected for non-linear summation (96). For histograms displaying
570 mEPSP amplitude frequencies, the same number of spontaneous events was analyzed for each NMJ
571 (per genotype or experimental condition). This ensured that no individual NMJs were overrepresented or
572 underrepresented in the aggregate analyses.

573 **Immunostaining and Image Analysis:** Third instar larvae were filleted in HL3 saline. Dissected animals
574 were fixed for 3 minutes in Bouin's fixative (Ricca Chemical Company, Arlington, TX), washed using
575 standard procedures, and incubated in primary antibodies overnight at 4°C. This was followed by

576 additional washes and a two-hour incubation in secondary antibody at room temperature. Staining was
577 performed using the following primary antibodies: mouse anti-GluRIIA (8B4D2) at 1:250 (bouton/cluster
578 counting) or 1:500 (intensity analyses) (Developmental Studies Hybridoma Bank (DSHB), University of
579 Iowa); rabbit anti-Dlg 1:30,000 (97, 98), mouse anti-Brp (nc82) 1:250 (32) (deposited to DSHB by
580 Buchner, E.), rabbit anti-GFP 1:250 (Torrey Pines Biolabs Inc. TP401). The following fluorophore-
581 conjugated antibodies were also used (Jackson ImmunoResearch Laboratories): goat anti-mouse-488
582 1:1000 (DyLight); and goat anti-rabbit-549 1:2000 (Dylight). Larval preparations were mounted in
583 Vectashield (Vector Laboratories) and imaged at room temperature using Zen software on a Zeiss 700
584 LSM mounted on an Axio Observer.Z1. An EC Plan-Neofluar 40X Oil DIC Objective (aperture 1.30) or an
585 EC Plan-Apochromat 63x Oil DIC Objective (aperture 1.40) (Carl Zeiss Microscopy) was used.

586 For analysis of fluorescence intensity and area, experimental and control larval preparations were
587 stained in the same container, mounted on the same slide, imaged using identical acquisition settings,
588 and analyzed using the same procedure and thresholds. Bouton and glutamate receptor cluster numbers
589 were quantified semi-automatically using the 'Spots' function in Imaris x64 v7.6.0 (Bitplane, Zurich
590 Switzerland). Any errors in automated counting were corrected by hand to arrive at the final value.
591 GluRIIA and Dlg levels were assessed using ImageJ 1.48s/Java 1.6.0_24 (64-bit) with Fiji plugins. Z-
592 stack images were compressed using the maximum projection function; ROIs were hand drawn to
593 exclude non-synaptic structures; a minimum threshold was set for each channel to eliminate background
594 fluorescence; and the Measure function was used to assess fluorescence intensity and area.

595 **Statistical Analyses and Data Plots:** Most electrophysiological comparisons were made across
596 multiple data sets. As appropriate, statistical significance was either assessed by one-way ANOVA with
597 Tukey's post-hoc analysis for multiple comparisons (Gaussian distribution), or a non-parametric Kruskal-
598 Wallis ANOVA with Dunn's post-hoc analysis for multiple comparisons (non-Gaussian distribution). Other
599 statistical tests utilized included Fisher's exact tests for viability counts or for statistical counts of gigantic
600 mEPSP events; Log-rank tests for survivability curves; linear regression analyses for calcium
601 cooperativity; and Student's T-Tests for direct comparisons between one control group and one

experimental group. p values of * $p < 0.05$, ** $p < 0.01$, *** $p < 0.001$, and **** $p < 0.0001$ were considered significant. The values reported or plotted on regular bar graphs are mean ± SEM. The values reported and plotted on box-and-whisker graphs are: box (25th – 75th percentiles), whiskers (1st – 99th percentiles), line (median), + symbol (average), and individual raw data points plotted outside the 1st and 99th percentiles. Raw values for mEPSP electrophysiological data are given in Table 1. Statistical analyses were performed in GraphPad Prism (GraphPad Software).

ACKNOWLEDGEMENTS: We thank Martin Müller, Chun-Fang Wu and members of the Frank lab for helpful comments on earlier versions of this manuscript, and the laboratories of Tina Tootle and Fang Lin for helpful discussions. We thank the Bloomington Drosophila Stock Center and the Vienna Drosophila Resource Center for several fly stocks detailed in the Materials and Methods section.

615 **REFERENCES**
616
617 1. Kullmann DM. Neurological channelopathies. Annu Rev Neurosci. 2010;33:151-72.

618 2. Russell JF, Fu YH, Ptacek LJ. Episodic neurologic disorders: syndromes, genes, and
619 mechanisms. Annu Rev Neurosci. 2013;36:25-50.

620 3. Ryan DP, Ptacek LJ. Episodic neurological channelopathies. Neuron. 2010;68(2):282-92.

621 4. Ophoff RA, Terwindt GM, Vergouwe MN, van Eijk R, Oefner PJ, Hoffman SM, et al. Familial
622 hemiplegic migraine and episodic ataxia type-2 are caused by mutations in the Ca2+ channel gene
623 CACNL1A4. Cell. 1996;87(3):543-52.

624 5. Kors EE, Terwindt GM, Vermeulen FL, Fitzsimons RB, Jardine PE, Heywood P, et al. Delayed
625 cerebral edema and fatal coma after minor head trauma: role of the CACNA1A calcium channel subunit
626 gene and relationship with familial hemiplegic migraine. Ann Neurol. 2001;49(6):753-60.

627 6. Pietrobon D. Calcium channels and migraine. Biochimica et biophysica acta. 2013;1828(7):1655-
628 65.

629 7. Eikermann-Haerter K, Dilekoz E, Kudo C, Savitz SI, Waeber C, Baum MJ, et al. Genetic and
630 hormonal factors modulate spreading depression and transient hemiparesis in mouse models of familial
631 hemiplegic migraine type 1. The Journal of clinical investigation. 2009;119(1):99-109.

632 8. van den Maagdenberg AM, Pietrobon D, Pizzorusso T, Kaja S, Broos LA, Cesetti T, et al. A
633 Cacna1a knockin migraine mouse model with increased susceptibility to cortical spreading depression.
634 Neuron. 2004;41(5):701-10.

635 9. van den Maagdenberg AM, Pizzorusso T, Kaja S, Terpolilli N, Shapovalova M, Hoebeek FE, et al.
636 High cortical spreading depression susceptibility and migraine-associated symptoms in Ca(v)2.1 S218L
637 mice. Ann Neurol. 2010;67(1):85-98.

638 10. Kaja S, van de Ven RC, Broos LA, Veldman H, van Dijk JG, Verschuuren JJ, et al. Gene dosage-
639 dependent transmitter release changes at neuromuscular synapses of CACNA1A R192Q knockin mice
640 are non-progressive and do not lead to morphological changes or muscle weakness. Neuroscience.
641 2005;135(1):81-95.

642 11. Kaja S, Van de Ven RC, Broos LA, Frants RR, Ferrari MD, Van den Maagdenberg AM, et al.
643 Severe and progressive neurotransmitter release aberrations in familial hemiplegic migraine type 1
644 Cacna1a S218L knock-in mice. Journal of neurophysiology. 2010;104(3):1445-55.

645 12. Di Guilmi MN, Wang T, Inchauspe CG, Forsythe ID, Ferrari MD, van den Maagdenberg AM, et al.
646 Synaptic gain-of-function effects of mutant Cav2.1 channels in a mouse model of familial hemiplegic
647 migraine are due to increased basal [Ca2+]i. J Neurosci. 2014;34(21):7047-58.

648 13. Inchauspe CG, Urbano FJ, Di Guilmi MN, Ferrari MD, van den Maagdenberg AM, Forsythe ID, et
649 al. Presynaptic CaV2.1 calcium channels carrying familial hemiplegic migraine mutation R192Q allow
650 faster recovery from synaptic depression in mouse calyx of Held. Journal of neurophysiology.
651 2012;108(11):2967-76.

652 14. Inchauspe CG, Urbano FJ, Di Guilmi MN, Forsythe ID, Ferrari MD, van den Maagdenberg AM, et
653 al. Gain of function in FHM-1 Cav2.1 knock-in mice is related to the shape of the action potential. Journal
654 of neurophysiology. 2010;104(1):291-9.

655 15. Hullugundi SK, Ansuini A, Ferrari MD, van den Maagdenberg AM, Nistri A. A hyperexcitability
656 phenotype in mouse trigeminal sensory neurons expressing the R192Q Cacna1a missense mutation of
657 familial hemiplegic migraine type-1. Neuroscience. 2014;266:244-54.

658 16. Park J, Moon H, Akerman S, Holland PR, Lasalandra MP, Andreou AP, et al. Differential
659 trigeminovascular nociceptive responses in the thalamus in the familial hemiplegic migraine 1 knock-in
660 mouse: a Fos protein study. Neurobiology of disease. 2014;64:1-7.

661 17. Pietrobon D, Moskowitz MA. Pathophysiology of migraine. Annu Rev Physiol. 2013;75:365-91.

662 18. Vecchia D, Tottene A, van den Maagdenberg AM, Pietrobon D. Abnormal cortical synaptic
663 transmission in CaV2.1 knockin mice with the S218L missense mutation which causes a severe familial
664 hemiplegic migraine syndrome in humans. Frontiers in cellular neuroscience. 2015;9:8.

665 19. Vecchia D, Tottene A, van den Maagdenberg AM, Pietrobon D. Mechanism underlying unaltered
666 cortical inhibitory synaptic transmission in contrast with enhanced excitatory transmission in CaV2.1
667 knockin migraine mice. Neurobiology of disease. 2014;69:225-34.

668 20. Inagaki A, Frank CA, Usachev YM, Benveniste M, Lee A. Pharmacological Correction of Gating
669 Defects in the Voltage-Gated Cav2.1 Ca(2+) Channel due to a Familial Hemiplegic Migraine Mutation.
670 Neuron. 2014;81(1):91-102.

671 21. Eikermann-Haerter K, Arbel-Ornath M, Yalcin N, Yu ES, Kuchibhotla KV, Yuzawa I, et al.
672 Abnormal synaptic Ca(2+) homeostasis and morphology in cortical neurons of familial hemiplegic
673 migraine type 1 mutant mice. Ann Neurol. 2015;78(2):193-210.

674 22. Kawasaki F, Zou B, Xu X, Ordway RW. Active zone localization of presynaptic calcium channels
675 encoded by the cacophony locus of Drosophila. J Neurosci. 2004;24(1):282-5.

676 23. Lin DM, Goodman CS. Ectopic and increased expression of Fasciclin II alters motoneuron growth
677 cone guidance. Neuron. 1994;13(3):507-23.

678 24. Brand AH, Perrimon N. Targeted gene expression as a means of altering cell fates and
679 generating dominant phenotypes. Development. 1993;118(2):401-15.

680 25. Breen TR, Lucchesi JC. Analysis of the dosage compensation of a specific transcript in
681 Drosophila melanogaster. Genetics. 1986;112(3):483-91.

682 26. Cline TW, Meyer BJ. Vive la difference: males vs females in flies vs worms. Annual review of
683 genetics. 1996;30:637-702.

684 27. Lucchesi JC, Kuroda MI. Dosage compensation in Drosophila. Cold Spring Harbor perspectives
685 in biology. 2015;7(5).

686 28. Fouquet W, Owald D, Wichmann C, Mertel S, Depner H, Dyba M, et al. Maturation of active zone
687 assembly by Drosophila Bruchpilot. J Cell Biol. 2009;186(1):129-45.

688 29. Frank CA, Kennedy MJ, Goold CP, Marek KW, Davis GW. Mechanisms underlying the rapid
689 induction and sustained expression of synaptic homeostasis. Neuron. 2006;52(4):663-77.

690 30. Frank CA, Pielage J, Davis GW. A presynaptic homeostatic signaling system composed of the
691 Eph receptor, ephexin, Cdc42, and CaV2.1 calcium channels. Neuron. 2009;61(4):556-69.

692 31. Gaviño MA, Ford KJ, Archila S, Davis GW. Homeostatic synaptic depression is achieved through
693 a regulated decrease in presynaptic calcium channel abundance. eLife. 2015;4.

694 32. Wagh DA, Rasse TM, Asan E, Hofbauer A, Schwenkert I, Durrbeck H, et al. Bruchpilot, a protein
695 with homology to ELKS/CAST, is required for structural integrity and function of synaptic active zones in
696 Drosophila. Neuron. 2006;49(6):833-44.

697 33. DiAntonio A, Petersen SA, Heckmann M, Goodman CS. Glutamate receptor expression regulates
698 quantal size and quantal content at the Drosophila neuromuscular junction. J Neurosci. 1999;19(8):3023-
699 32.

700 34. Feng Y, Ueda A, Wu CF. A modified minimal hemolymph-like solution, HL3.1, for physiological
701 recordings at the neuromuscular junctions of normal and mutant Drosophila larvae. Journal of
702 neurogenetics. 2004;18(2):377-402.

703 35. McGuire SE, Le PT, Osborn AJ, Matsumoto K, Davis RL. Spatiotemporal rescue of memory
704 dysfunction in Drosophila. Science. 2003;302(5651):1765-8.

705 36. Jan LY, Jan YN. Properties of the larval neuromuscular junction in Drosophila melanogaster. J
706 Physiol. 1976;262(1):189-214.

707 37. Martin AR. Quantal Nature of Synaptic Transmission. Physiol Rev. 1966;46:51-66.

708 38. Del Castillo J, Katz B. Quantal components of the end-plate potential. J Physiol. 1954;124(3):560-
709 73.

710 39. Frank CA. Homeostatic plasticity at the Drosophila neuromuscular junction. Neuropharmacology.
711 2014;78:63-74.

712 40. Frank CA. How voltage-gated calcium channels gate forms of homeostatic synaptic plasticity.
713 Frontiers in cellular neuroscience. 2014;8:40.

714 41. Brusich DJ, Spring AM, Frank CA. A single-cross, RNA interference-based genetic tool for
715 examining the long-term maintenance of homeostatic plasticity. Frontiers in cellular neuroscience.
716 2015;9:107.

717 42. Shortridge RD, Yoon J, Lending CR, Bloomquist BT, Perdew MH, Pak WL. A Drosophila
718 phospholipase C gene that is expressed in the central nervous system. J Biol Chem.
719 1991;266(19):12474-80.

720 43. Tedford HW, Zamponi GW. Direct G protein modulation of Cav2 calcium channels. Pharmacol
721 Rev. 2006;58(4):837-62.

722 44. Cremona O, De Camilli P. Phosphoinositides in membrane traffic at the synapse. Journal of cell
723 science. 2001;114(Pt 6):1041-52.

724 45. Goni FM, Alonso A. Structure and functional properties of diacylglycerols in membranes.
725 Progress in lipid research. 1999;38(1):1-48.

726 46. Huang FD, Woodruff E, Mohrmann R, Broadie K. Rolling blackout is required for synaptic vesicle
727 exocytosis. J Neurosci. 2006;26(9):2369-79.

728 47. Peters C, Bayer MJ, Buhler S, Andersen JS, Mann M, Mayer A. Trans-complex formation by
729 proteolipid channels in the terminal phase of membrane fusion. Nature. 2001;409(6820):581-8.

730 48. Rohrbough J, Broadie K. Lipid regulation of the synaptic vesicle cycle. Nat Rev Neurosci.
731 2005;6(2):139-50.

732 49. Wu L, Bauer CS, Zhen XG, Xie C, Yang J. Dual regulation of voltage-gated calcium channels by
733 PtdIns(4,5)P2. Nature. 2002;419(6910):947-52.

734 50. Dahdal D, Reeves DC, Ruben M, Akabas MH, Blau J. Drosophila pacemaker neurons require g
735 protein signaling and GABAergic inputs to generate twenty-four hour behavioral rhythms. Neuron.
736 2010;68(5):964-77.

737 51. Llano I, Gonzalez J, Caputo C, Lai FA, Blayney LM, Tan YP, et al. Presynaptic calcium stores
738 underlie large-amplitude miniature IPSCs and spontaneous calcium transients. Nat Neurosci.
739 2000;3(12):1256-65.

740 52. Liu Q, Chen B, Yankova M, Morest DK, Maryon E, Hand AR, et al. Presynaptic ryanodine
741 receptors are required for normal quantal size at the Caenorhabditis elegans neuromuscular junction. J
742 Neurosci. 2005;25(29):6745-54.

743 53. Collin T, Marty A, Llano I. Presynaptic calcium stores and synaptic transmission. Curr Opin
744 Neurobiol. 2005;15(3):275-81.

745 54. Emptage NJ, Reid CA, Fine A. Calcium stores in hippocampal synaptic boutons mediate short-
746 term plasticity, store-operated Ca2+ entry, and spontaneous transmitter release. Neuron.
747 2001;29(1):197-208.

748 55. Simkus CR, Stricker C. The contribution of intracellular calcium stores to mEPSCs recorded in
749 layer II neurones of rat barrel cortex. J Physiol. 2002;545(Pt 2):521-35.

750 56. Wong CO, Chen K, Lin YQ, Chao Y, Duraine L, Lu Z, et al. A TRPV channel in Drosophila motor
751 neurons regulates presynaptic resting Ca2+ levels, synapse growth, and synaptic transmission. Neuron.
752 2014;84(4):764-77.

753 57. Joshi R, Venkatesh K, Srinivas R, Nair S, Hasan G. Genetic dissection of itpr gene function
754 reveals a vital requirement in aminergic cells of Drosophila larvae. Genetics. 2004;166(1):225-36.

755 58. Conti R, Tan YP, Llano I. Action potential-evoked and ryanodine-sensitive spontaneous Ca2+
756 transients at the presynaptic terminal of a developing CNS inhibitory synapse. J Neurosci.
757 2004;24(31):6946-57.

758 59. Dunn TW, Syed NI. Ryanodine receptor-transmitter release site coupling increases quantal size
759 in a synapse-specific manner. The European journal of neuroscience. 2006;24(6):1591-605.

760 60. Gordon GR, Bains JS. Noradrenaline triggers multivesicular release at glutamatergic synapses in
761 the hypothalamus. J Neurosci. 2005;25(49):11385-95.

762 61. Sharma G, Vijayaraghavan S. Modulation of presynaptic store calcium induces release of
763 glutamate and postsynaptic firing. Neuron. 2003;38(6):929-39.

764 62. Dunn TW, McCamphill PK, Syed NI. Activity-induced large amplitude postsynaptic mPSPs at
765 soma-soma synapses between Lymnaea neurons. Synapse. 2009;63(2):117-25.

766 63. Dockendorff TC, Robertson SE, Faulkner DL, Jongens TA. Genetic characterization of the 44D-
767 45B region of the Drosophila melanogaster genome based on an F2 lethal screen. Molecular & general
768 genetics : MGG. 2000;263(1):137-43.

769 64. Hallcher LM, Sherman WR. The effects of lithium ion and other agents on the activity of myo-
770 inositol-1-phosphatase from bovine brain. J Biol Chem. 1980;255(22):10896-901.

771 65. Lenox RH, Wang L. Molecular basis of lithium action: integration of lithium-responsive signaling
772 and gene expression networks. Mol Psychiatry. 2003;8(2):135-44.

773 66. Gafni J, Munsch JA, Lam TH, Catlin MC, Costa LG, Molinski TF, et al. Xestospongins: potent
774 membrane permeable blockers of the inositol 1,4,5-trisphosphate receptor. Neuron. 1997;19(3):723-33.

775 67. Wilcox RA, Primrose WU, Nahorski SR, Challiss RA. New developments in the molecular
776 pharmacology of the myo-inositol 1,4,5-trisphosphate receptor. Trends Pharmacol Sci. 1998;19(11):467-
777 75.

778 68. Goswami SP, Bucurenciu I, Jonas P. Miniature IPSCs in hippocampal granule cells are triggered
779 by voltage-gated Ca2+ channels via microdomain coupling. J Neurosci. 2012;32(41):14294-304.

780 69. Ermolyuk YS, Alder FG, Surges R, Pavlov IY, Timofeeva Y, Kullmann DM, et al. Differential
781 triggering of spontaneous glutamate release by P/Q-, N- and R-type Ca2+ channels. Nat Neurosci.
782 2013;16(12):1754-63.

783 70. Xu-Friedman MA, Regehr WG. Maximinis. Nat Neurosci. 2000;3(12):1229-30.

784 71. Melom JE, Akbergenova Y, Gavornik JP, Littleton JT. Spontaneous and evoked release are
785 independently regulated at individual active zones. J Neurosci. 2013;33(44):17253-63.

786 72. Yao WD, Wu CF. Auxiliary Hyperkinetic beta subunit of K+ channels: regulation of firing
787 properties and K+ currents in Drosophila neurons. J Neurophysiol. 1999;81(5):2472-84.

788 73. Berke BA, Lee J, Peng IF, Wu CF. Sub-cellular Ca2+ dynamics affected by voltage- and Ca2+-
789 gated K+ channels: Regulation of the soma-growth cone disparity and the quiescent state in Drosophila
790 neurons. Neuroscience. 2006;142(3):629-44.

791 74. Gao Z, Todorov B, Barrett CF, van Dorp S, Ferrari MD, van den Maagdenberg AM, et al.
792 Cerebellar ataxia by enhanced Ca(V)2.1 currents is alleviated by Ca2+-dependent K+-channel activators
793 in Cacna1a(S218L) mutant mice. J Neurosci. 2012;32(44):15533-46.

794 75. Vanmolkot KR, Kors EE, Turk U, Turkdogan D, Keyser A, Broos LA, et al. Two de novo mutations
795 in the Na,K-ATPase gene ATP1A2 associated with pure familial hemiplegic migraine. European journal
796 of human genetics : EJHG. 2006;14(5):555-60.

797 76. Bergquist S, Dickman DK, Davis GW. A hierarchy of cell intrinsic and target-derived homeostatic
798 signaling. Neuron. 2010;66(2):220-34.

799 77. Lee J, Ueda A, Wu CF. Pre- and post-synaptic mechanisms of synaptic strength homeostasis
800 revealed by slowpoke and shaker K+ channel mutations in Drosophila. Neuroscience. 2008;154(4):1283-
801 96.

802 78. Lee J, Ueda A, Wu CF. Distinct roles of Drosophila cacophony and Dmca1D Ca(2+) channels in
803 synaptic homeostasis: genetic interactions with slowpoke Ca(2+) -activated BK channels in presynaptic
804 excitability and postsynaptic response. Developmental neurobiology. 2014;74(1):1-15.

805 79. Peng IF, Wu CF. Drosophila cacophony channels: a major mediator of neuronal Ca2+ currents
806 and a trigger for K+ channel homeostatic regulation. J Neurosci. 2007;27(5):1072-81.

807 80. Parrish JZ, Kim CC, Tang L, Bergquist S, Wang T, Derisi JL, et al. Kruppel mediates the selective
808 rebalancing of ion channel expression. Neuron. 2014;82(3):537-44.

809 81. Li P, Chen SR. Molecular basis of Ca(2)+ activation of the mouse cardiac Ca(2)+ release channel
810 (ryanodine receptor). The Journal of general physiology. 2001;118(1):33-44.

811 82. Rahman T. Dynamic clustering of IP3 receptors by IP3. Biochemical Society transactions.
812 2012;40(2):325-30.

813 83. Zahradnik I, Gyorke S, Zahradnikova A. Calcium activation of ryanodine receptor channels--
814 reconciling RyR gating models with tetrameric channel structure. The Journal of general physiology.
815 2005;126(5):515-27.

816 84. Laver DR. Ca2+ stores regulate ryanodine receptor Ca2+ release channels via luminal and
817 cytosolic Ca2+ sites. Clinical and experimental pharmacology & physiology. 2007;34(9):889-96.

818 85. de Vries B, Eising E, Broos LA, Koelewijn SC, Todorov B, Frants RR, et al. RNA expression
819 profiling in brains of familial hemiplegic migraine type 1 knock-in mice. Cephalalgia : an international
820 journal of headache. 2014;34(3):174-82.

821 86. Drissi H, Lasmoles F, Le Mellay V, Marie PJ, Lieberherr M. Activation of phospholipase C-beta1
822 via Galphaq/11 during calcium mobilization by calcitonin gene-related peptide. J Biol Chem.
823 1998;273(32):20168-74.

824 87. Morara S, Wang LP, Filippov V, Dickerson IM, Grohovaz F, Provini L, et al. Calcitonin gene-
825 related peptide (CGRP) triggers Ca2+ responses in cultured astrocytes and in Bergmann glial cells from
826 cerebellar slices. Eur J Neurosci. 2008;28(11):2213-20.

827 88. Drissi H, Lieberherr M, Hott M, Marie PJ, Lasmoles F. Calcitonin gene-related peptide (CGRP)
828 increases intracellular free Ca2+ concentrations but not cyclic AMP formation in CGRP receptor-positive
829 osteosarcoma cells (OHS-4). Cytokine. 1999;11(3):200-7.

830 89. Goadsby PJ, Edvinsson L, Ekman R. Release of vasoactive peptides in the extracerebral
831 circulation of humans and the cat during activation of the trigeminovascular system. Ann Neurol.
832 1988;23(2):193-6.

833 90. Goadsby PJ, Edvinsson L, Ekman R. Vasoactive peptide release in the extracerebral circulation
834 of humans during migraine headache. Ann Neurol. 1990;28(2):183-7.

835 91. Kaiser EA, Russo AF. CGRP and migraine: could PACAP play a role too? Neuropeptides.
836 2013;47(6):451-61.

837 92. Hazelrigg T, Levis R, Rubin GM. Transformation of white locus DNA in drosophila: dosage
838 compensation, zeste interaction, and position effects. Cell. 1984;36(2):469-81.

839 93. Deshpande M, Venkatesh K, Rodrigues V, Hasan G. The inositol 1,4,5-trisphosphate receptor is
840 required for maintenance of olfactory adaptation in Drosophila antennae. J Neurobiol. 2000;43(3):282-8.

841 94. Dietzl G, Chen D, Schnorrer F, Su KC, Barinova Y, Fellner M, et al. A genome-wide transgenic
842 RNAi library for conditional gene inactivation in Drosophila. Nature. 2007;448(7150):151-6.

843 95. Davis GW, DiAntonio A, Petersen SA, Goodman CS. Postsynaptic PKA controls quantal size and
844 reveals a retrograde signal that regulates presynaptic transmitter release in Drosophila. Neuron.
845 1998;20(2):305-15.

846 96. Martin AR. A further study of the statistical composition on the end-plate potential. J Physiol.
847 1955;130(1):114-22.

848 97. Budnik V, Koh YH, Guan B, Hartmann B, Hough C, Woods D, et al. Regulation of synapse
849 structure and function by the Drosophila tumor suppressor gene dlg. Neuron. 1996;17(4):627-40.

850 98. Pielage J, Cheng L, Fetter RD, Carlton PM, Sedat JW, Davis GW. A presynaptic giant ankyrin
851 stabilizes the NMJ through regulation of presynaptic microtubules and transsynaptic cell adhesion.
852 Neuron. 2008;58(2):195-209.

853

854 **FIGURE LEGENDS**

855

856 **Figure 1: SL- and DM-expressing flies exhibit coarse phenotypes. (A)** Schematic of Ca_V2-type
857 calcium channel α1a subunit, with substitutions to Drosophila Cacophony (Cac) residues indicated
858 (mammalian numbering in parentheses) and a CLUSTAL-Omega alignment of Cac, human CACNA1A,
859 and mouse CACNA1A amino acids spanning the relevant region ([*] - fully conserved residue; [:] -
860 strongly similar; [.] - weakly similar). **(B-C)** Visible phenotypes for larvae resulting from crosses of
861 *elaV(C155)-Gal4* females x *Balancer Chrom*/*UAS-cac*$^{MUT\ or\ WT}$ males. **(B)** Premature spiracle protrusion in
862 larvae expressing the *UAS-cac*^{SL} (shown) or *UAS-cac*^{DM} (not shown) transgenic lines. The spiracle
863 phenotype does not occur in larvae expressing *UAS-cac*^{RQ} or *UAS-cac*^{WT}. **(C)** Same crosses as in (B)
864 showing diminished *UAS-cac* mutant viability. "*UAS-cac* Viability Index" = # *UAS-cac* transgenic adult
865 progeny/# Balancer Chromosome siblings, normalized to 100% for WT female progeny counts (see
866 Table 1 for raw progeny counts; for all *UAS-cac* comparisons, $n \geq 115$ Balancer sibling progeny were
867 counted). Male and female progeny were considered separately due to possible sex differences. *** $p <$
868 0.001 by Fisher's Exact test compared to WT sex-specific control. # $p = 0.05$, ### $p < 0.001$ by Fisher's
869 Exact test between sexes for the SL or DM genotypes. **(D, E)** For both males and females, there was
870 starkly diminished longevity for adult flies expressing the DM transgene. **** $p < 0.0001$ by Log-rank test.

871

872 **Figure 2: Neuronal expression and synaptic localization of Cac-GFP are normal. (A-D)** Images of
873 larval central nervous systems for animals expressing Cac-GFP WT or mutant transgenes. Anti-GFP
874 (red), and anti-Bruchpilot (Brp - green) staining are shown. Scale bar 100 μm. **(E)** Per unit area in
875 neurons, there is no significant difference in neuronal Cac-GFP intensity across the transgenic lines (*ns* –
876 not significant, $p = 0.50$ by one-way ANOVA, and $p > 0.6$ for all possible Tukey's post-hoc comparisons).
877 **(F-I)** Transgenic Cac-GFP proteins successfully localize to NMJ active zones, as indicated by co-staining
878 with anti-Brp (green) and anti-GFP (red). Scale bar 5 μm. **(J)** For DM-expressing NMJs, synaptic bouton
879 numbers are normal, except for slight undergrowth for synapse A2 muscle 6/7 (* $p < 0.05$, Student's T-

880 test vs. WT, $n \geq 8$ NMJs for all genotypes and segments). **(K)** The number of glutamate receptor clusters
881 per synapse at DM-expressing NMJs is not statistically different than WT-expressing NMJs ($p > 0.1$,
882 Student's T-test, $n \geq 8$ NMJs for all genotypes and segments). **(L-M)** For DM-expressing NMJs, there is a
883 small increase in GluRIIA-containing receptor area coverage (L) and for anti-GluRIIA staining intensity
884 normalized for anti-Dlg intensity (M) (* $p < 0.05$ by Student's T-test vs. WT for both measures, $n \geq 15$
885 NMJs for each genotype).

886

887 **Figure 3: SL- and DM-expressing flies display hyperexcitability in evoked neurotransmission. (A)**
888 Average EPSP amplitudes at 0.4 mM $[Ca^{2+}]_e$. for non-transgenic control (w^{1118}) or various Cac-GFP-
889 expressing lines (** $p < 0.01$ by one-way ANOVA with Tukey's post-hoc vs. w^{1118}; # $p < 0.05$ and ### $p <$
890 0.001 vs. WT; $n \geq 12$ for all genotypes,). **(B)** Average quantal content (QC estimated as EPSP/mEPSP)
891 at 0.4 mM $[Ca^{2+}]_e$ ($p > 0.15$ by one-way ANOVA with Tukey's post-hoc for all genotypes, compared to
892 both w^{1118} and WT controls). **(C)** Log-log plots of extracellular calcium concentration vs. QC corrected for
893 non-linear summation (NLS QC). There are no statistically significant differences in calcium cooperativity
894 between genotypes ($p = 0.16$ by linear regression analysis). **(D, E)** Example electrophysiological traces
895 of **(D)** normal and **(E)** abnormal EPSP waveforms. **(F)** Effect of genotype on EPSP waveforms in
896 response to 30 presynaptic pulses: normal, extra discharge, and shoulders categories. "RQ only"
897 signifies larvae with a null endogenous *cac* mutation rescued to viability by the RQ-expressing
898 transgene. **(G)** Effect of genotype on number of extra discharges observed per 30 presynaptic pulses (* p
899 < 0.05 and *** $p < 0.001$ vs. WT by one-way Kruskal-Wallis ANOVA with Dunn's post-hoc). **(H)**
900 Penetrance and **(I)** severity of DM-associated extra discharge waveform dysfunction in low extracellular
901 Mg^{2+} (6 mM). All genotypes abbreviated (WT, DM, SL, RQ) are *elaV(C155)-Gal4/Y; UAS-cac-eGFP*$^{(X)}$/+
902 or w^{1118} for non-transgenic wild type. Data bars represent the average value and error bars the SEM.

903

904 **Figure 4: SL- and DM-expressing NMJs have enhanced mEPSPs. (A)** Electrophysiological traces of
905 spontaneous activity at WT- and DM-expressing NMJs. Example traces with two different scales are
906 shown to display the variable severity of spontaneous neurotransmission phenotypes. **(B)** Effects of
907 genotype on average mEPSP amplitude. ** $p < 0.01$ vs. w^{1118} by one-way ANOVA with Tukey's post-hoc;
908 # $p < 0.05$, ### $p < 0.001$ vs. WT by one-way ANOVA with Tukey's post-hoc. **(C)** Effects of genotype on
909 mEPSP frequency. ### $p < 0.001$ vs. WT by one-way ANOVA with Tukey's post-hoc; $n \geq 12$ NMJs, all
910 genotypes. **(D)** Box and whisker plots of mEPSP amplitude range at 0.5 mM extracellular Ca^{2+}. Box
911 denotes 25th-75th percentile; line denotes median; + sign denotes average; whiskers range from 1st-99th
912 percentile; individual data points outside the 1st and 99th percentiles are also plotted; (*** $p < 0.001$ by
913 Kruskal-Wallis ANOVA with Dunn's post-hoc vs. either w^{1118} or WT; $n > 1400$ mEPSPs for each
914 genotype). **(E)** Cumulative probability histogram of the same data as (D) showing a marked rightward
915 shift in mEPSP amplitudes for SL- and DM-expressing NMJs. **(F)** Box and whisker plot (data as in (D)) of
916 mEPSP amplitude range when expressing the DM transgene for acute periods of developmental time
917 (*** $p < 0.001$ by Kruskal-Wallis ANOVA with Dunn's post-hoc vs. DM 0 hr, ### $p < 0.001$ by vs. DM 24
918 hr; $n > 1095$ mEPSPs for each genotype). **(G)** Cumulative probability histogram of the same data in (F)
919 showing a rightward shift in mEPSP amplitudes for longer periods of DM expression.

920

921 **Figure 5: Gigantic spontaneous events vanish in response to diminished Ca^{2+}, buffered Ca^{2+}, or**
922 **blocked Na_V function. (A)** Box and whisker plot of mEPSP amplitudes at 0.2 mM extracellular Ca^{2+}. Plot
923 as in Fig. 4 (*** $p < 0.001$ by Kruskal-Wallis ANOVA with Dunn's post-hoc vs. either w^{1118} or WT; $n > 780$
924 mEPSPs for each genotype). **(B)** Cumulative probability histogram of the same data as (A) showing a
925 rightward shift in mEPSP amplitudes for SL- and DM-expressing NMJs – but less so than for 0.5 mM
926 Ca^{2+} in Figure 4. **(C-E)** Cumulative probability histograms of mEPSP size separately showing the effects
927 of zero extracellular Ca^{2+} (C); application of BAPTA-AM in 0.5 mM Ca^{2+} (D); application of TTX in 0.5 mM
928 Ca^{2+} (E). For each case, the rightward shift in mEPSP size distribution persists due to DM expression.
929 However, the gigantic spontaneous events are eliminated (arrowheads). **(F)** Box and whisker plots

930 demonstrating elimination of gigantic spontaneous events. *** $p < 0.001$ by Fisher's exact test examining
931 the incidence of gigantic mEPSPs > 10 mV vs. DM or SL alone, as appropriate).

932

933 **Figure 6: Failure analysis - SL- and DM-expressing NMJs show elevated release probability at**
934 **very low extracellular calcium. (A-B)** Frequencies of evoked amplitudes at very low extracellular Ca^{2+}
935 (0.14 mM) for **(A)** WT-expressing NMJs and **(B)** DM-expressing NMJs. For the DM-expressing NMJs,
936 there is a clear rightward shift in the size distribution of DM-expressing events, as well as a marked
937 decrease in the frequency of failures (categorized as 0 mV events). **(C)** Further lowering extracellular
938 Ca^{2+} (0.1 mM) for DM reveals a leftward shift in size distribution and an increase in failure percentage
939 compared to (B). **(D)** For WT-, DM-, and SL-expressing NMJs, the average EPSP size for successfully
940 evoked events, as well as estimated QC for by failure analyses (0.14 mM Ca^{2+}). * $p < 0.05$; ** $p < 0.01$ by
941 one-way ANOVA with Tukey's post-hoc compared to WT. **(E)** Box and whisker plots for both failure
942 analysis and spontaneous events. Data are presented as in Figures 4 and 5 – this time showing the size
943 distributions of spontaneous mEPSP events (WT, DM, SL), as well as failure analysis (FA) evoked
944 events for the same genotypes (failures excluded).

945

946 **Figure 7: Inhibition of an intracellular Ca^{2+} release pathway dampens gain-of-function phenotypes**
947 **associated with FHM1-mimicking mutations. (A)** Schematic of an RNA interference (RNAi)-based
948 approach to identify suppressors of gain-of-function electrophysiological phenotypes. **(B)** Knockdown of
949 *Plc21C* gene function reverses the increase in spontaneous mEPSP amplitude elicited by DM
950 expression. **(C)** Box and whisker plots (as before) and **(D-E)** cumulative probability histograms (as
951 before) demonstrate that heterozygous, loss-of-function point mutations in genes encoding the IP_3
952 receptor ($Itpr^{\mu g3}$) and the Ryanodine receptor (RyR^{E4340K}) also diminish the gain-of-function spontaneous
953 mEPSP phenotypes in DM-expressing NMJs. *** $p < 0.001$ by Kruskal-Wallis ANOVA with Dunn's
954 multiple comparisons test vs. DM alone. **(F)** The RyR^{E4340K} mutation also diminishes evoked EPSP

955 hyperexcitability phenotypes in a DM-expressing background (# of extra discharges [ED] per muscle –
956 see also Figure 3).

957

958 **Figure 8: Pharmacological inhibition of intracellular Ca2+ release dampens gain-of-function**
959 **phenotypes associated with FHM1-mimicking mutations. (A-C)** Data displayed and analyzed as
960 before. Box and whisker plots (A) and cumulative probability histograms (B-C) demonstrate that acute
961 application of either LiCl (to block PIP_2 recycling) or Xestospongin C (to block IP_3 receptors) both
962 suppress the gain-of-function spontaneous mEPSP phenotypes in DM-expressing NMJs. *** $p < 0.001$
963 by Kruskal-Wallis ANOVA with Dunn's multiple comparisons test vs. DM alone. **(D)** Cartoon model
964 depicting neuronal components implicated in this study of regulating neurophysiology downstream of
965 migraine-mimicking amino-acid substitutions. Red – Ca_V2 channels; gray – IP_3 receptors; blue –
966 Ryanodine receptors; yellow – Na_V channels.

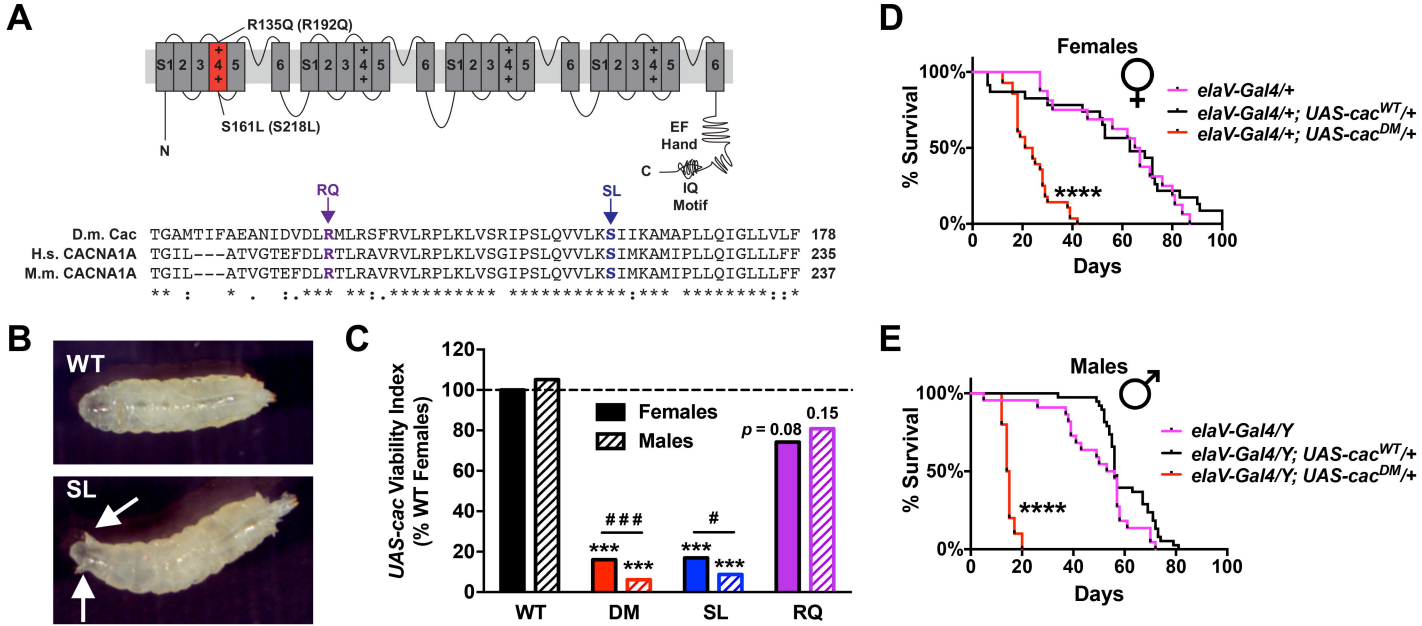
A
R135Q (R192Q)
S1 2 3 4 5 6 S1 2 3 4 5 6 S1 2 3 4 5 6 S1 2 3 4 5 6
S161L (S218L)
N
EF Hand
C
IQ Motif
RQ
SL
D.m. Cac TGAMTIFAEANIDVDLRMLRSFRVLRPLKLVSRIPSLQVVLKSIIKAMAPLLQIGLLVLF 178
H.s. CACNA1A TGIL---ATVGTEFDLRTLRAVRVLRPLKLVSGIPSLQVVLKSIMKAMIPLLQIGLLLFF 235
M.m. CACNA1A TGIL---ATVGTEFDLRTLRAVRVLRPLKLVSGIPSLQVVLKSIMKAMIPLLQIGLLLFF 237
B
WT
SL
C
UAS-cac Viability Index (% WT Females)
Females
Males
p = 0.08
0.15
###
#
***
WT
DM
SL
RQ
D
Females
% Survival
Days
elaV-Gal4/+
elaV-Gal4/+; UAS-cacWT/+
elaV-Gal4/+; UAS-cacDM/+
****
E
Males
% Survival
Days
elaV-Gal4/Y
elaV-Gal4/Y; UAS-cacWT/+
elaV-Gal4/Y; UAS-cacDM/+
****

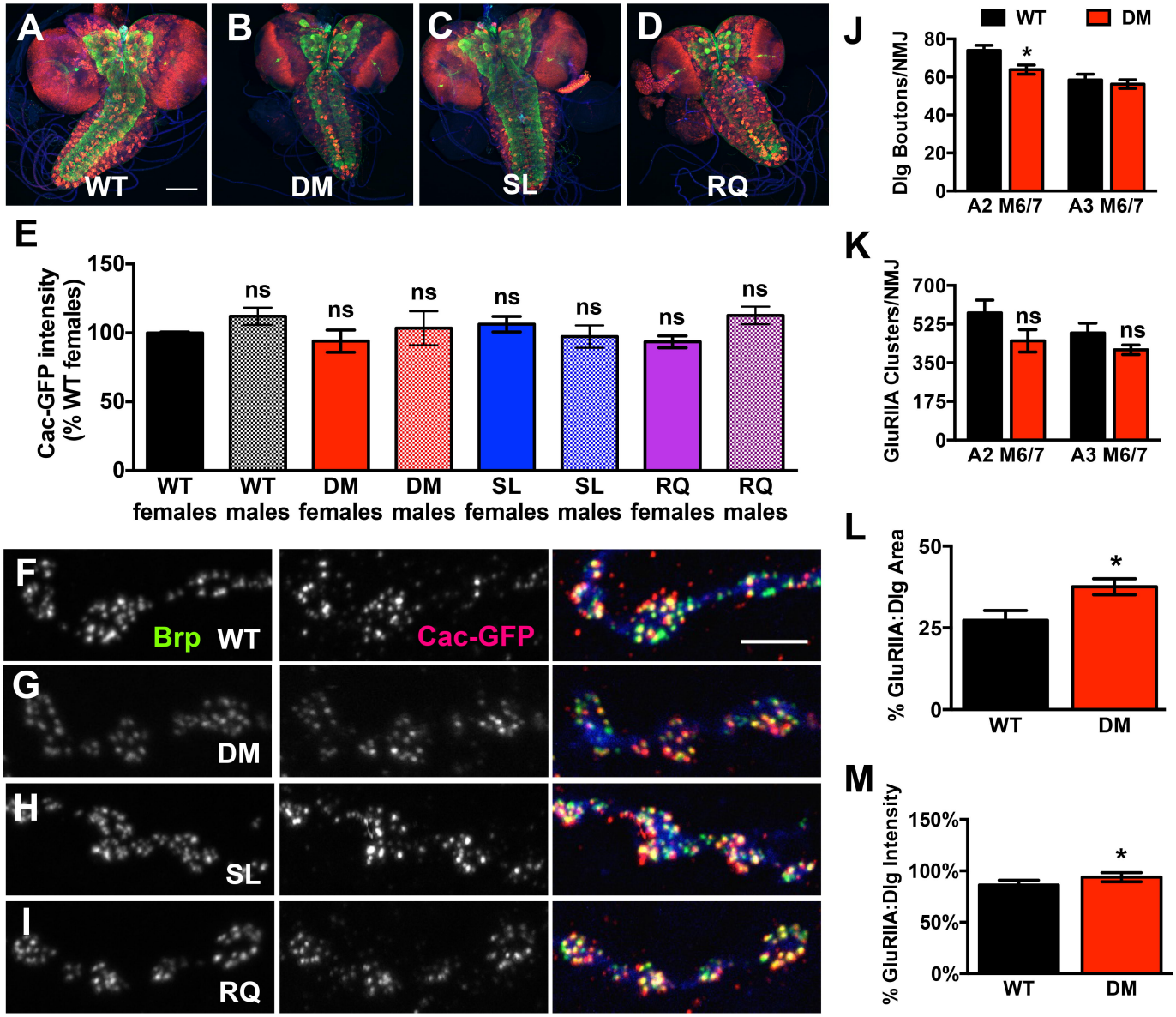
A
WT
B
DM
C
SL
D
RQ
J
WT
DM
Dlg Boutons/NMJ
80
60
40
20
0
*
A2 M6/7
A3 M6/7
E
Cac-GFP intensity
(% WT females)
150
100
50
0
ns
WT
females
WT
males
DM
females
DM
males
SL
females
SL
males
RQ
females
RQ
males
K
GluRIIA Clusters/NMJ
700
525
350
175
0
ns
A2 M6/7
A3 M6/7
F
Brp
WT
Cac-GFP
G
DM
H
SL
I
RQ
L
% GluRIIA:Dlg Area
50
25
0
*
WT
DM
M
% GluRIIA:Dlg Intensity
150%
100%
50%
0%
*
WT
DM

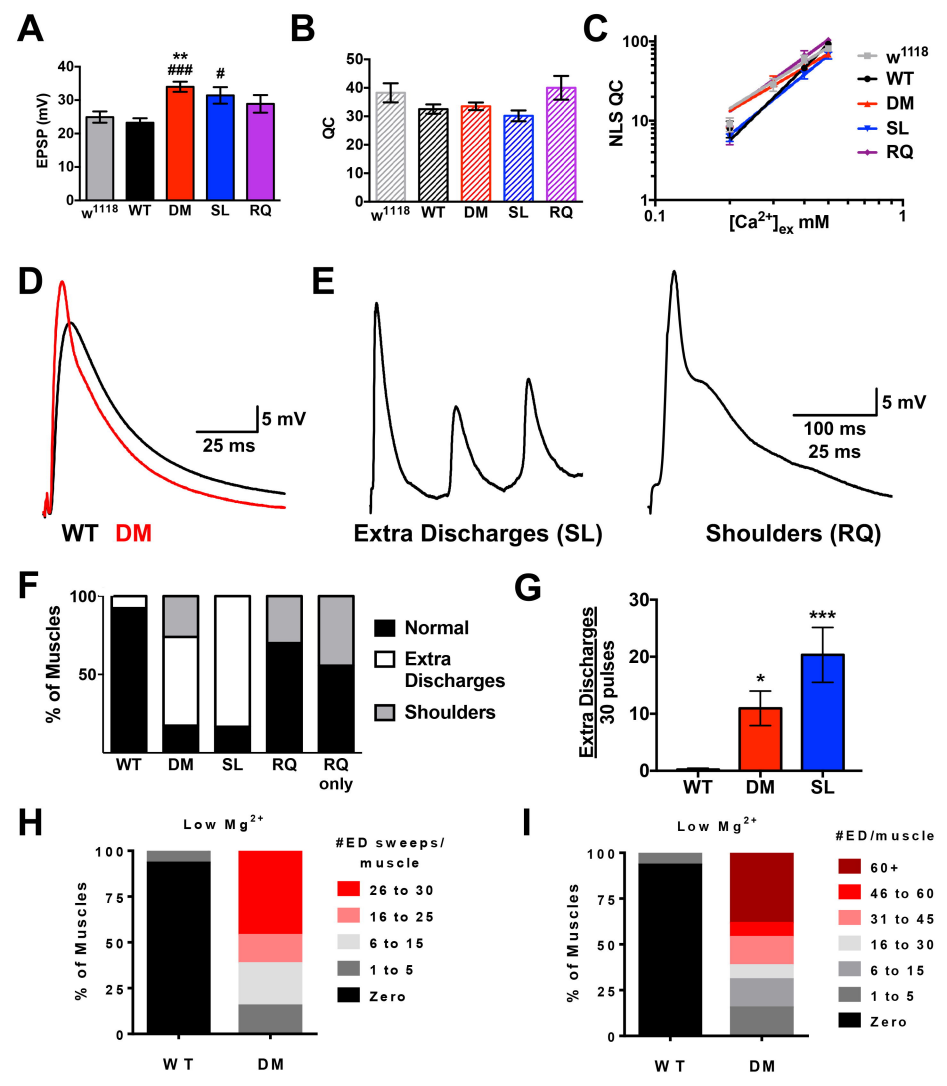
A
EPSP (mV)
40
30
20
10
0
**
###
#
w1118
WT
DM
SL
RQ
B
QC
50
40
30
20
10
0
w1118
WT
DM
SL
RQ
C
NLS QC
100
10
1
0.1
1
[Ca2+]ex mM
w1118
WT
DM
SL
RQ
D
5 mV
25 ms
WT
DM
E
Extra Discharges (SL)
5 mV
100 ms
25 ms
Shoulders (RQ)
F
% of Muscles
100
50
WT
DM
SL
RQ
RQ only
Normal
Extra Discharges
Shoulders
G
Extra Discharges / 30 pulses
30
20
10
0
*
***
WT
DM
SL
H
Low Mg2+
% of Muscles
100
75
50
25
0
W T
DM
#ED sweeps/ muscle
26 to 30
16 to 25
6 to 15
1 to 5
Zero
I
Low Mg2+
% of Muscles
100
75
50
25
0
W T
DM
#ED/muscle
60+
46 to 60
31 to 45
16 to 30
6 to 15
1 to 5
Zero

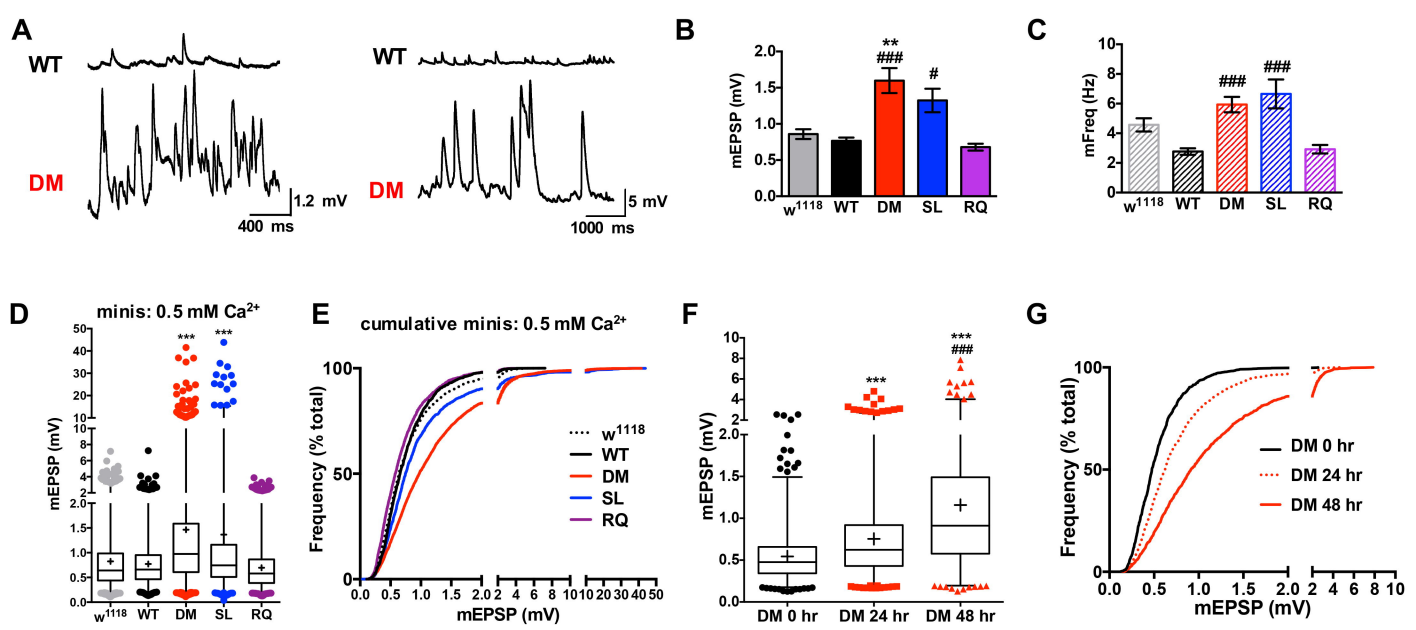
A
WT
DM
1.2 mV
400 ms
WT
DM
5 mV
1000 ms
B
mEPSP (mV)
**
###
#
w1118
WT
DM
SL
RQ
C
mFreq (Hz)
###
###
w1118
WT
DM
SL
RQ
D
minis: 0.5 mM Ca2+
mEPSP (mV)
***
***
w1118
WT
DM
SL
RQ
E
cumulative minis: 0.5 mM Ca2+
Frequency (% total)
mEPSP (mV)
w1118
WT
DM
SL
RQ
F
mEPSP (mV)
***
***
###
DM 0 hr
DM 24 hr
DM 48 hr
G
Frequency (% total)
mEPSP (mV)
DM 0 hr
DM 24 hr
DM 48 hr

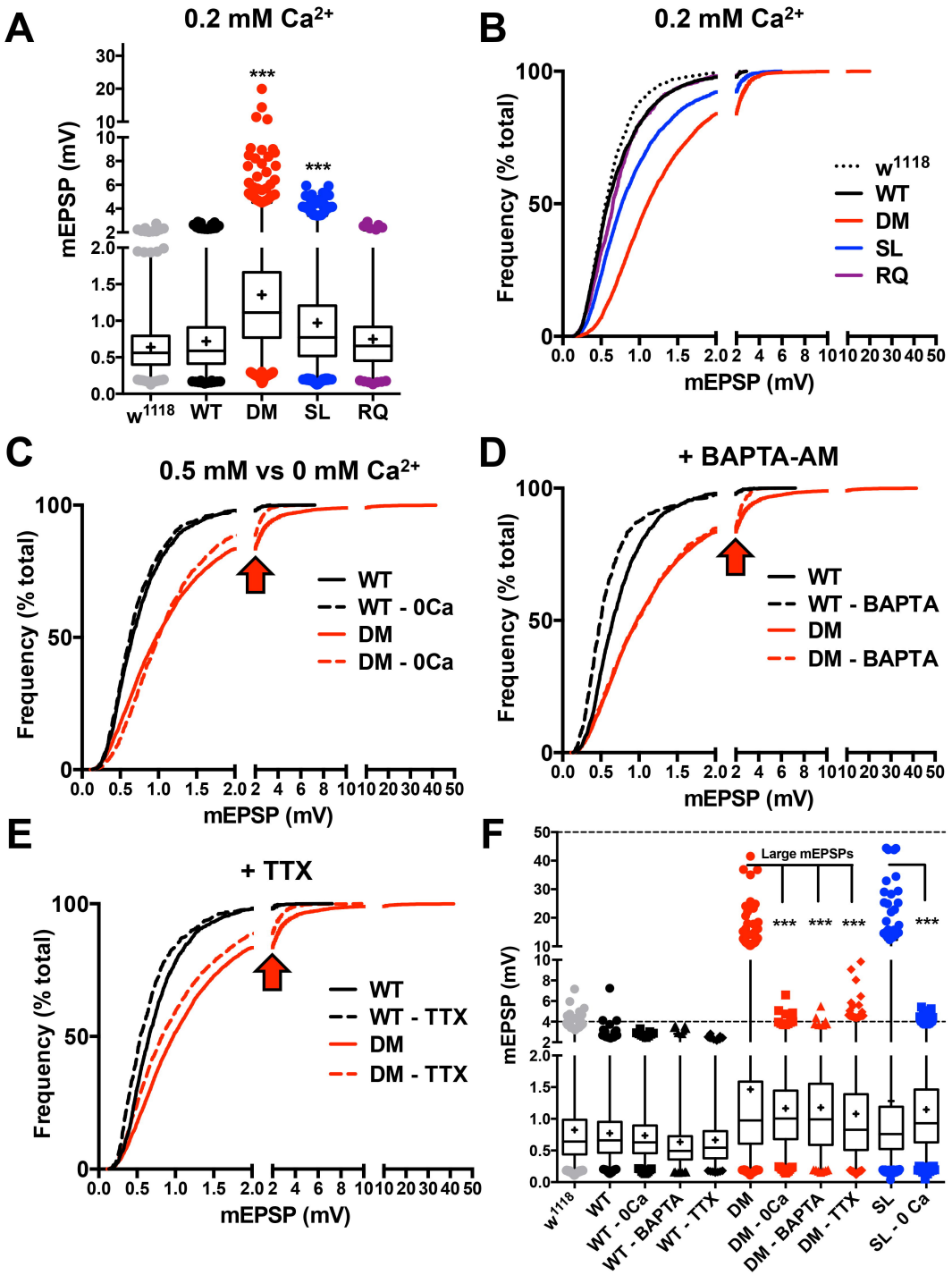
A
0.2 mM Ca2+
mEPSP (mV)
***
***
w1118
WT
DM
SL
RQ
B
0.2 mM Ca2+
Frequency (% total)
mEPSP (mV)
w1118
WT
DM
SL
RQ
C
0.5 mM vs 0 mM Ca2+
Frequency (% total)
mEPSP (mV)
WT
WT - 0Ca
DM
DM - 0Ca
D
+ BAPTA-AM
Frequency (% total)
mEPSP (mV)
WT
WT - BAPTA
DM
DM - BAPTA
E
+ TTX
Frequency (% total)
mEPSP (mV)
WT
WT - TTX
DM
DM - TTX
F
Large mEPSPs
mEPSP (mV)
w1118
WT
WT - 0Ca
WT - BAPTA
WT - TTX
DM
DM - 0Ca
DM - BAPTA
DM - TTX
SL
SL - 0 Ca

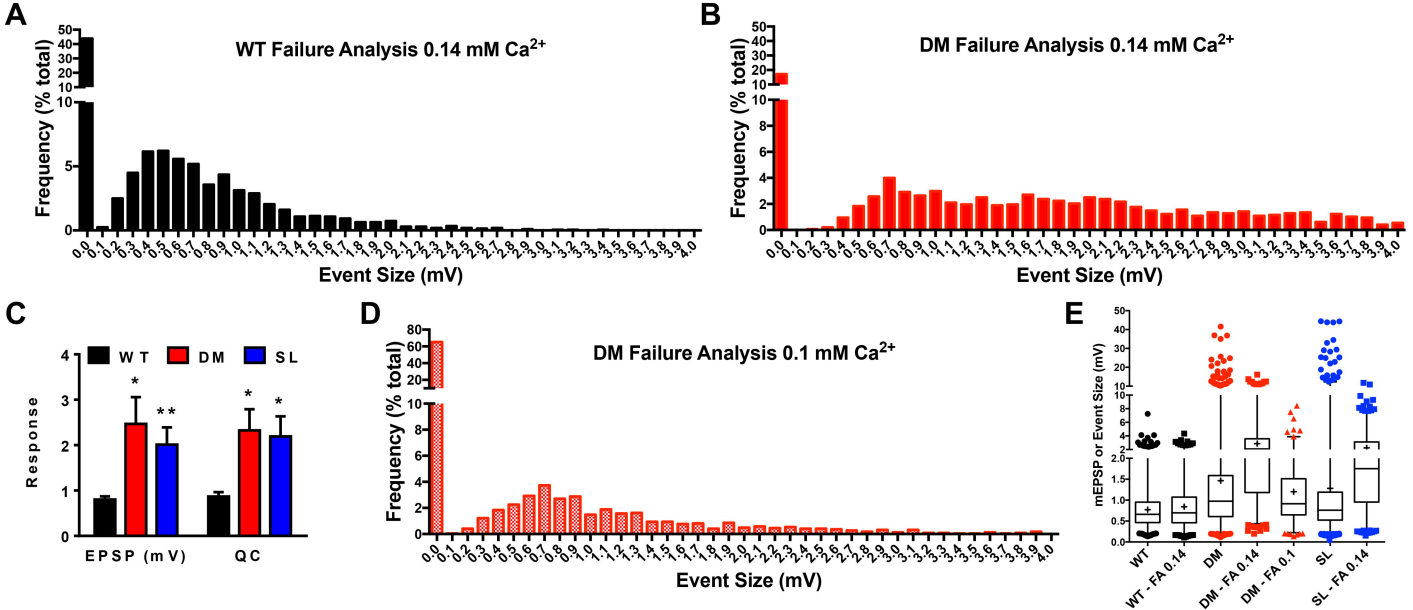
A
WT Failure Analysis 0.14 mM Ca2+
Frequency (% total)
Event Size (mV)
B
DM Failure Analysis 0.14 mM Ca2+
Frequency (% total)
Event Size (mV)
C
WT
DM
SL
Response
EPSP (mV)
QC
D
DM Failure Analysis 0.1 mM Ca2+
Frequency (% total)
Event Size (mV)
E
mEPSP or Event Size (mV)
WT
WT - FA 0.14
DM
DM - FA 0.14
DM - FA 0.1
SL
SL - FA 0.14

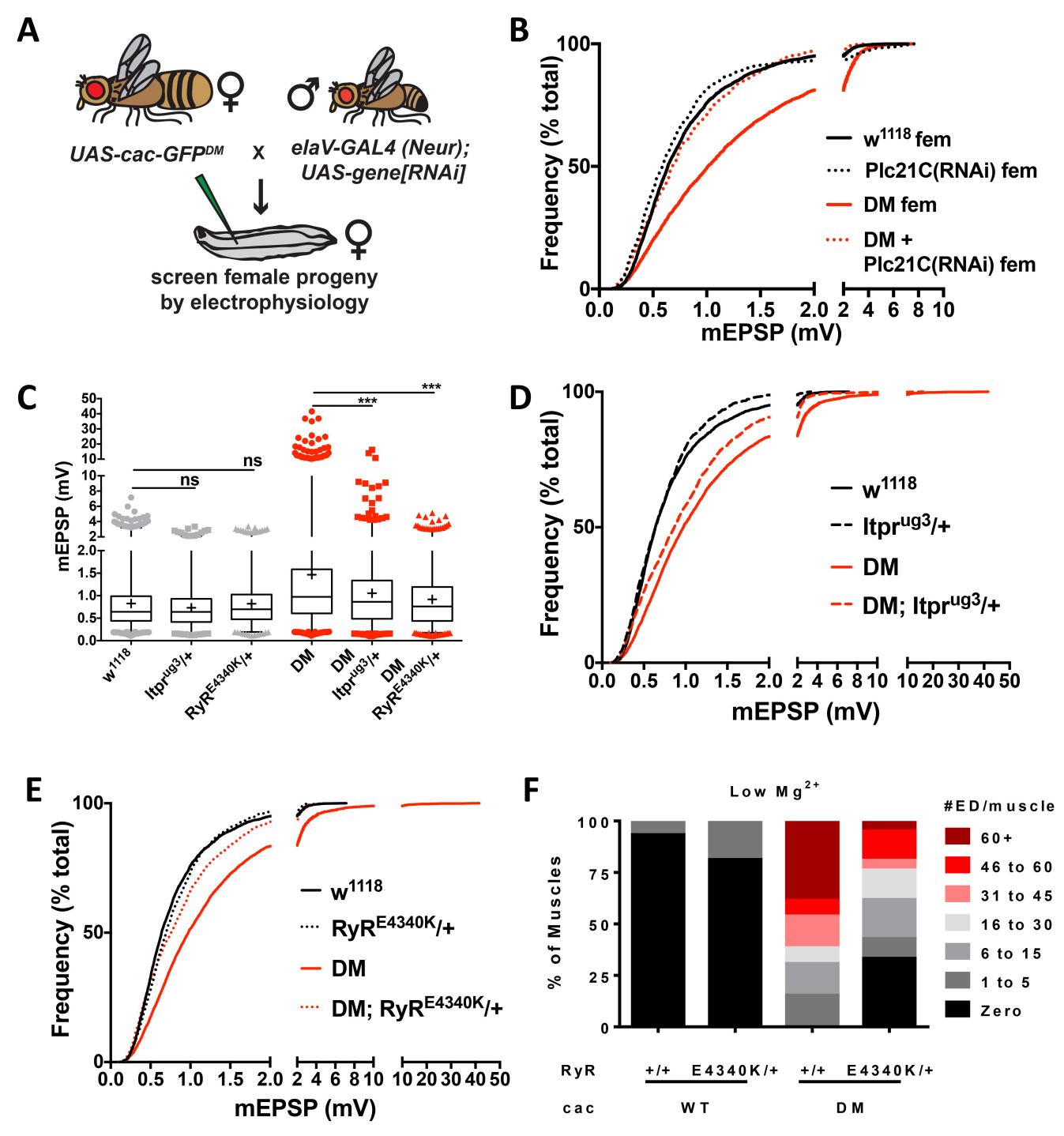
A
UAS-cac-GFP^DM
x
elaV-GAL4 (Neur);
UAS-gene[RNAi]
screen female progeny
by electrophysiology
B
Frequency (% total)
mEPSP (mV)
w1118 fem
Plc21C(RNAi) fem
DM fem
DM +
Plc21C(RNAi) fem
C
mEPSP (mV)
ns
ns
***
***
w1118
Itpr ug3/+
RyR E4340K/+
DM
DM
Itpr ug3/+
DM
RyR E4340K/+
D
Frequency (% total)
mEPSP (mV)
w1118
Itpr ug3/+
DM
DM; Itpr ug3/+
E
Frequency (% total)
mEPSP (mV)
w1118
RyR E4340K/+
DM
DM; RyR E4340K/+
F
Low Mg2+
% of Muscles
#ED/muscle
60+
46 to 60
31 to 45
16 to 30
6 to 15
1 to 5
Zero
RyR
+/+
E4340K/+
+/+
E4340K/+
cac
WT
DM

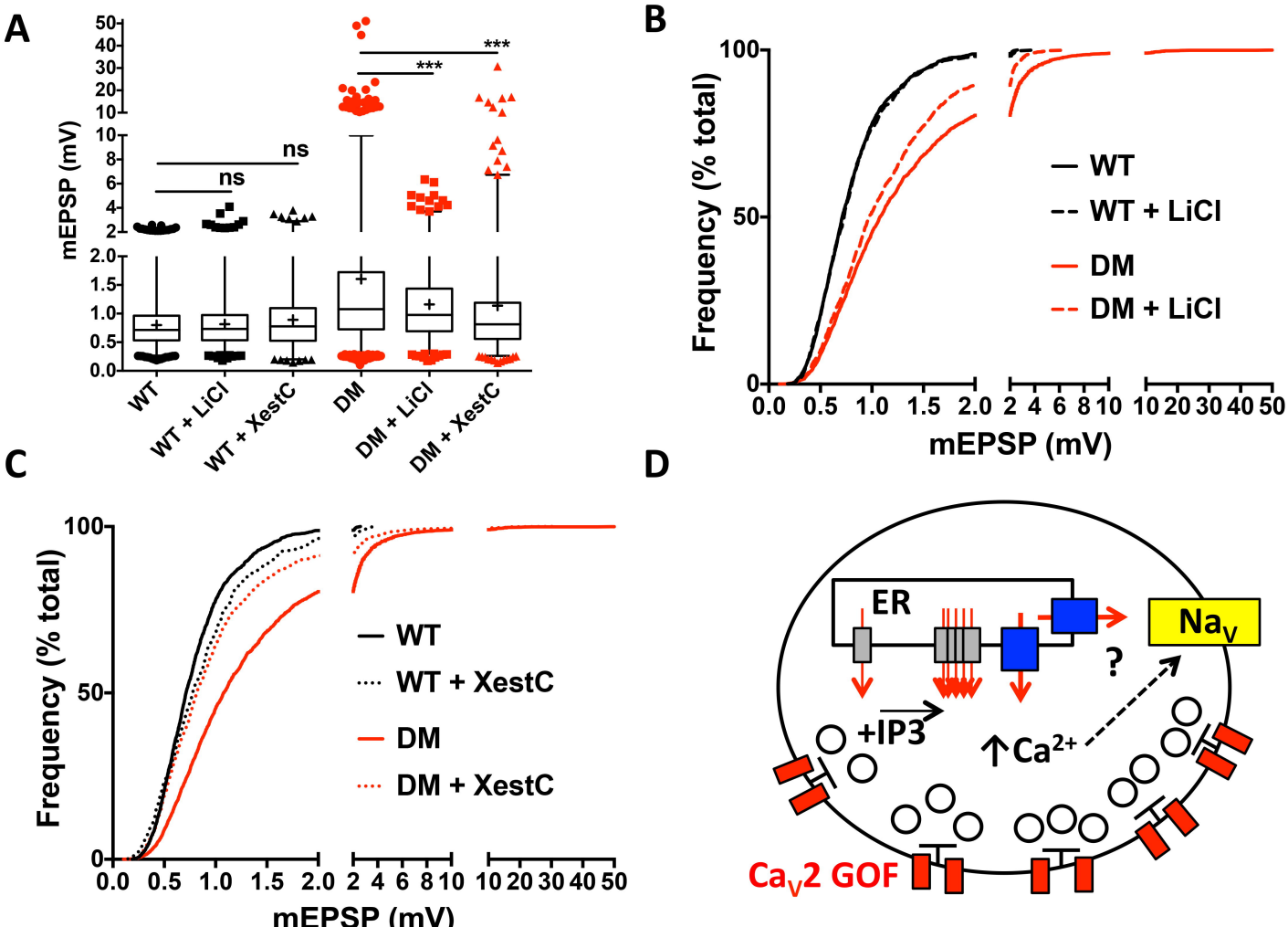
A
mEPSP (mV)
ns
ns
***
***
WT
WT + LiCl
WT + XestC
DM
DM + LiCl
DM + XestC
B
Frequency (% total)
mEPSP (mV)
WT
WT + LiCl
DM
DM + LiCl
C
Frequency (% total)
mEPSP (mV)
WT
WT + XestC
DM
DM + XestC
D
ER
Na$_V$
?
+IP3
↑Ca^{2+}
Ca$_V$2 GOF